University of Glasgow
DEPARTMENT OF
AEROSPACE
ENGINEERING

A Flow Visualization Study of a Pitching Delta Wing

G.U. Aero. Report 9824
R.B. Green

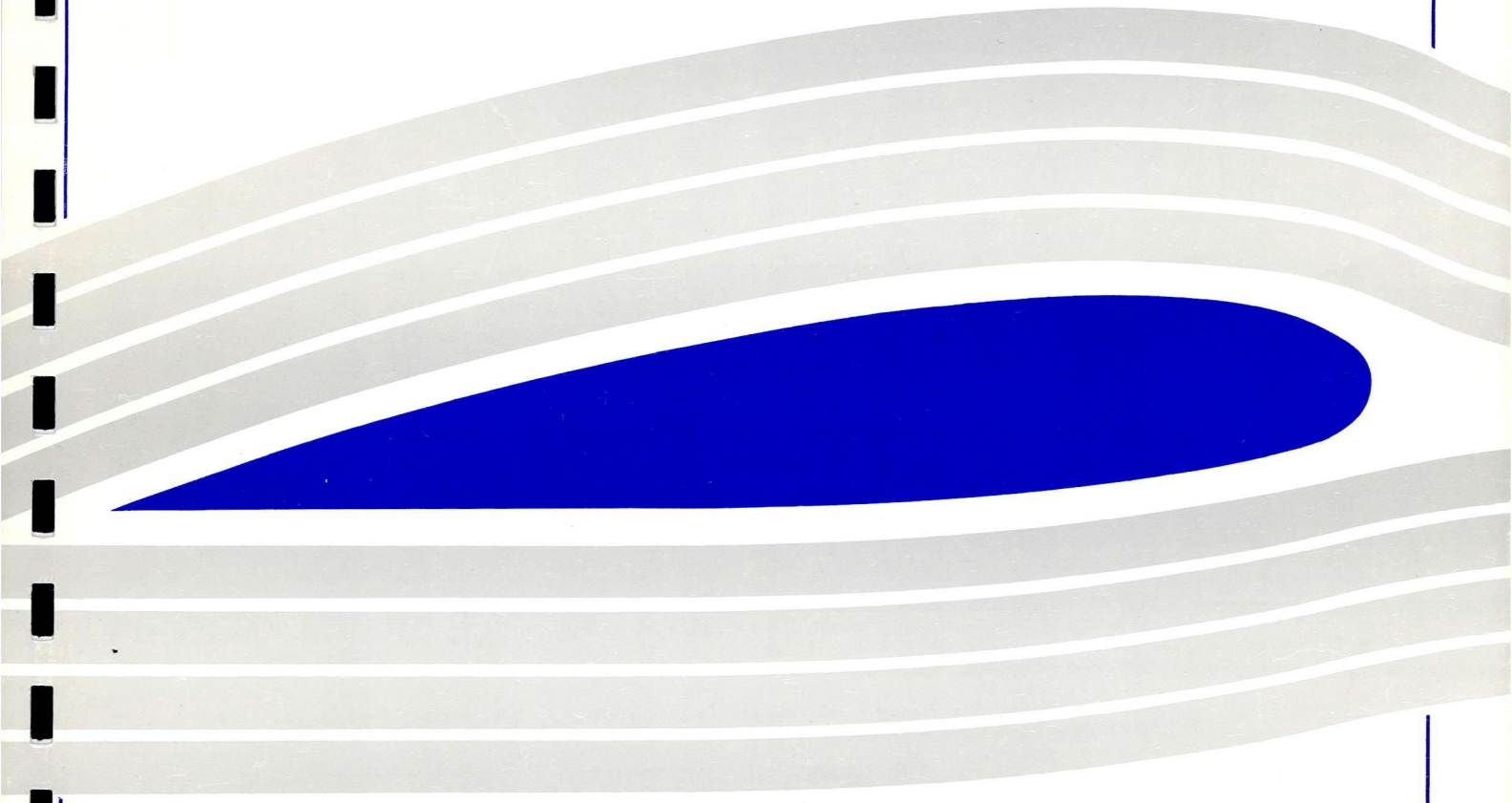

A Flow Visualization Study of a Pitching Delta Wing

G.U. Aero. Report 9824
R.B. Green

A FLOW VISUALIZATION STUDY OF A PITCHING DELTA WING

by

R.B. Green
Department of Aerospace Engineering
University of Glasgow
GLASGOW
G12 8QQ

Summary

A series of flow visualization tests of a uniformly pitching, 60° sweep delta wing have been performed. Measurements of vortex position over the wing and vortex breakdown are then presented. For the pitch up case, the vortex forms further outboard and closer to the wing surface than in the steady case, and vortex breakdown occurs at higher incidence. Vortex breakdown is preceded by a distortion of the vortex core. The pitch down case is characterized by the restoration of the vortex, the main effect being that a broken down flow is observed at lower incidence than the static case.

Nomenclature

c	model chord
k	reduced pitch rate ($\omega c/2U$)
Re	root chord Reynolds number
s	wing local semi-span
U	free stream speed
u_b	vortex breakdown progression speed
u_r	vortex restoration progression speed
x	chordwise position
x_b	chordwise vortex breakdown position
x_r	chordwise vortex restoration position
y_v	vortex height
z_v	vortex spanwise position
α	model incidence (deg)
ω	model pitch rate (radians s^{-1})

Contents

1.1 General introduction

Since the 1950s the aerodynamics of delta wings have provided an important research focus for both fundamental reasons and practical requirements of high performance aircraft design. In recent years additional impetus has been provided by the need for future generations of combat aircraft to be able to exhibit good manoeuvrability at high angle of attack (for reviews see Ashley et al. (1991), Erickson (1995)). Continued study of delta wing aerodynamics becomes important not only for direct application to the lifting and control surfaces, but also in the use of vortex generators to effect flow control and to address problems such as buffet.

Delta wing aerodynamics differ from flows over other wing planforms in that above relatively low incidence the flow field is dominated by separation from the wing leading edge. The most notable result of this is the formation of vortices over the lee surface of the wing, and these vortices are responsible for the generation of lift well beyond incidences at which more conventional wing planforms have stalled. Loss of lift and changes in the pitching moment characteristics are experienced when the vortices burst at high incidence. In the pitching wing case, the lift continues to increase until the vortex bursts (Ashley et al. (1991)). Burst therefore is of great importance in limiting the performance of a delta wing, and hence a knowledge of its behaviour is important for development of a flight control system for a manouevrable aircraft using a delta wing planform or other vortex generating control surfaces.

Vortex burst is characterized by a rapid transition from a well-organised, coherent vortex core to a relatively poorly defined rotational structure and large scale turbulence. Classically the vortex core may suddenly begin to follow a spiral trajectory (spiral mode) or may abruptly diverge (bubble mode) (Harvey (1960)). Stagnation within the vortex core occurs and the flow becomes highly unsteady. To compliment these descriptions, topological descriptions of the flow field indicate that there is a change from a stable to an unstable focus (i.e. from vortex stretching to vortex compression) above a critical angle (Magness et al. (1993)). In addition Lin & Rockwell (1995) identified intense regions of negative azimuthal vorticity during vortex burst after pitching motion to high incidence, indicating an azimuthal instability. Extensive measurements of vortex burst in a variety of wind tunnels, water channels and water tanks, and for a variety of leading edge shapes and model Reynolds numbers have indicated that vortex burst in the non-pitching case is most sensitive to the details of the model geometry (Lowson & Riley (1995)). While the phenomenon of burst has been extensively investigated for static delta wings (reviewed by Lowson & Riley (1995)), relatively few investigations have taken place on pitching wings (e.g. Rediniotis et al. (1994), Gursul & Yang (1995), Miau et al. (1992), Visbal (1994), LeMay et al. (1990), Hudson et al (1989), Parker (1977)). All of these investigations agree on the effect of pitching motion to delay progression of burst along the wing, although results describing the exact manner of burst progression differ. In view of Lowson & Riley's (1995) comments, any additional information on vortex burst behaviour on a pitching wing is useful.

Many investigations have determined the aerodynamic coefficient variations for a pitching delta wing (Ashley et al. (1991)). These have focussed upon the hysteretic load behaviour between the upstroke and downstroke of the wing motion, and have revealed little information regarding burst itself. To reveal the fluid mechanics of burst a satisfactory measurement system must be able to detect both the spatial and temporal changes that occur during burst. Flow visualization studies reveal qualitative changes, and have contributed a great deal to the understanding of vortex burst over non-pitching wings (e.g. Lowson (1991)). For pitching wings a number of studies have been performed (e.g. Wolffelt (1986), Miau et al. (1992) and Hudson et al. (1989)), and these have provided information on the rate of burst progression. Laser Doppler Velocimetry and velocity probe measurements provide a great deal of information regarding the flow but only at one point in space (Honkan & Andreapoulos (1997), Cornelius, K.C. (1995), Miau et al. (1992), Rediniotis et al. (1994)). Particle Image Velocimetry has been used by Lin & Rockwell (1995) among others, and provides information for a slice of the flow field, but obtaining temporal information is difficult owing to the nature of the photographic methods employed. Therefore, these methods will not supply readily the necessary spatial and temporal information for the quantification of the whole unsteady flow field over the pitching delta wing. An additional problem is that since they are field measurement methods they will be impractical to implement as a burst sensor to provide feedback information representing the state of the flow for a flight control scheme. However the use of sufficient pressure tappings placed over enough of the lee surface of the wing will give information indicating the state of the flow field (Greenwell & Wood (1992)) and are practical to include in a flight control system. Most studies using pressure measurements have focussed upon small parts of the wing or have been of low spatial resolution (Gursul & Yang (1995), Rediniotis et al. (1994)). The few studies that have taken place using high resolution surface pressure measurements have quantified changes in the spanwise pressure distribution associated with burst (Greenwell & Wood (1992)), and in the few cases where unsteady pressure data are available the post-breakdown characteristics of the flow have been described (Vaughan & Wood (1995)). Even so, these studies have tended to rely upon measurements taken at a single spatial location or a small number of locations, and the surface pressure information is built up over a series of tests via phase-locked conditional sampling. In order to address this difficulty, recent experiments at Glasgow have used a 60° sweep delta wing instrumented with up to 200 surface mounted pressure transducers (Jupp et al (1998)). Using a 200 channel data logger capable of a sampling rate of 50kHz per channel, therefore, the development of the instantaneous surface pressure field during almost any desired pitching motion was measured. The model containing the pressure transducers was specially designed for the tests. In view of Lowson & Riley's (1995) comments regarding burst incidences reported by various investigators, it was appreciated that the burst incidences would be unique to the particular model shape used in the pressure data tests. To assist with the interpretation of the data from the pressure instrumented model, it was therefore a priority that a comprehensive flow visualization study of the particular model shape was performed, and this provided the basic motivation for the present flow visualization study. Delta wing aerodynamics has been

shown to be relatively insensitive to Reynolds number, so the flow visualization study could be performed in a more suitable facility than the wind tunnel used for the pressure tests. Therefore the Department's Low Speed Flow Visualization wind tunnel would be used, and the tests would supply information regarding the burst behaviour during pitching motion. In addition a PIV study using the same facility would provide more detailed flow field information than the flow visualization study could provide.

The following report describes the results of the flow visualization phase of the study, which was initiated using funds provided by the Nuffield foundation. The delay in vortex breakdown for the pitch up case compared to the non-pitching case has been assessed, and the vortex behaviour during pitching motion is described. In addition studies of the wing performing a pitch down motion are described, and the importent differences between this case and the non-pitching case are discussed.

1.2 Scope of the current work

The original proposal to the Nuffield Foundation, from which the present work followed, is shown in appendix A. The goals were to perform a quality flow visualization of a pitching delta wing and then to perform a PIV based study of the flow field. The former has been achieved, although the PIV study has not yet been successful. The main reason for this is that the power of the laser available at the outset of the research ultimately proved to be insufficient for images of adequate quality for PIV. Particle traces on a photographic emulsion were obtained using microspheres, although this was achieved with only a very small illumination area, which meant that photographing the whole flow field would prove to be problematic. In addition seeding a non-return tunnel with 10μm particles proved to be an unacceptable health risk. The most important result from this aspect of the work, however, is that the author then pursued funding for more powerful equipment with a PIV study of delta wing vortex flows as the main subject of investigation. The author has since acquired two pulsed Nd:YAG lasers (one is capable of double pulsing itself), a beam combination unit and other optics, a digital video camera with a double exposure/ double image capability, a frame grabber and computing equipment for image processing. The total value of this equipment is some £90,000. A number of the above items were eventually used as part of the present flow visualization study. The PIV capability is currently being built up, however, and no data were available at the time of writing of this report. The equipment purchased from the Nuffield Foundation grant is central to the additional investigations to take place.

1.3 Items purchased from Nuffield Foundation grant

The original proposal was for an octagonal mirror for use in PIV measurements, a motor and controller for model actuation and a PC. The grant awarded was £3000, which was less than the sum requested. Together with assistance from the Department, a 150MHz PC was purchased together with a Panasonic A.C. digital servo motor. The motor has a peak torque capability of 7Nm and a maximum

rotational speed of 3000rpm, and will be suitable for use in a number of the Department's wind tunnels. Optics, materials for model manufacture and some photographic consumables were also paid for from the grant.

1.4 Other work performed using equipment purchased from Nuffield Foundation grant

The author has been involved with a number of other research projects in the Department during the period of the current grant. Funding shortfalls mean that Departmental equipment allocations are stretched. Therefore the motor and PC purchased from the current grant were used to assist with the experimentation in a Blade Vortex Interaction project funded by the EPSRC (grant GR/K 13547). The motor was used to remotely position a vortex generator in the wind tunnel, and its use served as a convenient familiarization and debugging exercise. Remote positioning of the vortex generator drastically cut down the wind tunnel time for the experimentation, which allowed many more runs than were previously planned to be performed. This contributed to the successful outcome of the test programme.

2. Experimental method

In this section details are given of the wind tunnel, model and measurement methodology.

2.1 The flow visualization wind tunnel

The experiments were conducted in the 0.9m by 0.9m flow visualization wind tunnel at the University of Glasgow. A schematic diagram is shown in figure 1. The working section is housed inside a sealed room. A fan is placed at the downstream end of the working section, so that when the fan runs air is sucked through the 9:1 contraction and down the working section. The air then passes into another sealed room and back out into the atmosphere through filters. The maximum working speed is approximately $2ms^{-1}$. Smoke was generated by a C.F. Taylor Scientific smoke generator. This consisted of a heating unit, which vapourized Shell Ondina oil, and a CO_2 supply which pumped the smoke out of the smoke generator.

2.2 Model details

Lowson & Riley's (1995) survey of experimental delta wing results indicated that model geometry was the most significant factor in determining the position of vortex breakdown. Hence the geometry of the present model had to reflect that of the model used in the pressure tests. In addition since the Reynolds number in the smoke tunnel would be much lower than the pressure data tests anyway, the smoke tunnel model size could be determined on the basis of matching the model span to tunnel width ratio. The smoke tunnel model was therefore an exact 43.25% scale replica of the model used in the pressure data tests. A diagram of the model is shown in figure 2.

The sweep angle was 60° and the model was constructed from aluminium. The model had a flat leeward surface and a shaped windward surface, and the sharp leading edges were bevelled at 20°. The root chord length was 346mm. The overall thickness to chord ratio was 9%. To visualize the flow the method of Lowson (1991) was adopted. In this method smoke was injected out of a narrow slot 0.5mm below the leeward surface running parallel to the leading edge. An almost continuous sheet of smoke was therefore generated which infected the shear layer springing from the leading edge.

A schematic diagram of the model pitching mechanism is shown in figure 3. The model was supported at the quarter chord point by a strut fixed to the tunnel floor. Pitching motion was achieved using a 40mm pitch ball screw and flange nut mechanism. The flange nut was attached to the model trailing edge by a series of linkages. The screw was rotated by the Panasonic 750W digital A.C. servo motor purchased from the current grant; in order that the motor ran at a stable speed, a 5:1 reduction gear box was placed between the motor and screw shafts. As the screw turned, the flange nut was constrained to move up and down the screw by the linear bearing and shaft.

The model motion was controlled using the IBM compatible PC purchased from the present grant. The PC was fitted with a National Instruments LAB-PC+ general purpose data acquisition card. This card has a number of bi-directional digital ports, three programmable counters, eight analogue input channels and two analogue output channels. The card was programmed using LabVIEW software; the motor was operated in velocity control mode, so one analogue output channel of the card was used to generate a waveform proportional to the required motor speed. This waveform accounted for the geometry of the pitching mechanism, with the intention that the model performed the required pitching motion.

2.3 Flow visualization methodology

At the outset of the research period the only illumination source available was a 0.5W Argon laser. This was ideal for direct visual inspection of the flow, but its low power proved to be problematic for good quality photography. The availability of the Nd:YAG laser later in the research was therefore a considerable bonus. This laser is a Spectra Physics GCR-130-10 with a maximum output energy of some 250mJ at 532nm (green). The repetition rate is 10Hz and the pulse duration is 8ns. Suitable optics created a light sheet which could be positioned in a vertical plane anywhere over the model surface.

A number of options were available for photographing the flow patterns. These were video recording the flow, or photography using a 35mm camera. Unless the model is pitching very slowly and the flow phenomena do not evolve rapidly video photography is not a suitable option, as the relatively poor spatial resolution and interlacing effect lead to poor quality pictures (particularly with the pulsed Nd:YAG laser). The initial thrust was therefore to use a 35mm camera combined with the Nd:YAG laser. A Nikon F70 camera was available for this purpose. It was therefore essential that care was taken to correctly synchronize

the camera, the model motion and the pulsed laser, and this was achieved as follows.

(i) The laser was to be operated in Q-switch mode, since this results in a much more brilliant pulse of light. The laser flash lamp must run continuously. With the laser in single shot mode an output pulse of light may be generated on demand subject to the 10Hz flash lamp rate; this means that the actual laser pulse may occur 0.1s after it was required, and this forms the crux of the synchronization problem.

(ii) A fire signal to the laser controller ensures that the laser Q-switch is fired at the next available flash lamp pulse. The laser control unit supplies a 5V output pulse train synchronous with the flash lamp. Hence to pulse the laser at a specified model incidence, the model motion must be synchronized with the flash lamp pulse train such that a flash lamp pulse occurred as the model passed the specified incidence. This was achieved by padding the start of the model control waveform with zeroes (i.e. zero speed), and synchronizing the start of the waveform generation with the laser flash lamp signal using the counters on the PC data acquisition card.

(iii) The signal to trigger the Q-switch firing sequence itself could be supplied at up to 0.1s before the actual laser pulse. In practice this signal was a 5V pulse supplied by the second analogue output channel on the PC data acquisition card; the pulse drove a fast TTL relay, which created the required short circuit for firing the Q-switch. Measurement of the camera shutter opening delay with a fast photo-diode indicated that the camera shutter took some 0.22 s to open. The camera shutter was therefore opened by an earlier TTL pulse on the same channel as the laser fire pulse. The entire camera shutter control and laser trigger voltage waveform was constructed in the LabVIEW control software and was generated synchronously with the motor control voltage waveform. A complete timing diagram is shown in figure 4. Measurement of the synchronization with a digital oscilloscope indicated that the laser pulse occurred to within 0.25° of the required model incidence; this error was basically due to the discretization of the motor control and laser fire waveforms.

Additional hardware acquired during the period of the research was a Kodak Megaplus ES1.0 digital video camera and Imaging Technology IC-PCI digital frame grabber. This camera has the advantage over a conventional video camera in that its resolution is high (1k by 1k pixels) and it is a progressive scan camera. This camera was far more suitable then the 35mm camera for the flow visualization since the images were available instantly, and therefore as soon as it was available it was used in preference to the 35mm camera. Use of this equipment required an additional PC; a 300MHz Pentium II was used, and the frame grabber was installed in one of the PCI slots of the PC. Synchronization of the digital camera with the laser was essentially identical to the 35mm camera case, except that since the response of the digital camera shutter was very fast the open camera shutter pulse ahead of the laser fire pulse was not required. Actual camera triggering was performed with the aid of a National Instruments PC-TIO-10 counter-timer card, programmed by LabVIEW and installed in the same PC as

the frame grabber. The digital camera required a TTL pulse, which was provided by the counter-timer card. A timing diagram for triggering the digital video camera is shown in figure 5. The counter-timer card was programmed to wait for the laser trigger signal from the laser fire control signal (described above). As soon as this signal was detected, one counter was armed to provide a 1MHz timebase source, and another counter was enabled to provide a 1ms long pulse, 20μs after the leading edge of each laser flash lamp pulse (this 20μs delay was timed using the 1MHz source). The frame grabber was then armed. At the next flash lamp pulse, which is the required laser pulse, the camera shutter was therefore triggered. The overall result was that camera was actually triggered some 100μs before the laser pulse itself. A second flash lamp pulse created another camera trigger signal which cleared the grab wait status on the IC-PCI frame grabber. As soon as this happened the two counters were disarmed so that the camera trigger was disabled, and the image was transferred from the frame grabber memory to the PC memory. The digital camera and frame grabber were programmed using LabVIEW with the IMAQ image processing library. The facility to capture up to 20 frames at a rate of up to 5 frames per second was included in the LabVIEW software; the start of the frame acquire sequence was as described above, although the two counters that synchronized the frame capture to the laser flash lamp were not disabled until the entire frame capture sequence was completed.

3. Results

For all the tests the wind tunnel was set at a speed of $0.42ms^{-1}$. This gave a nominal root chord based Reynolds number of 10000. For the pitching case the model performed a constant pitch rate "ramp" test in either the positive ("ramp-up" from low to high incidence) or negative ("ramp-down" from high to low incidence) directions. Reduced pitch rates of 0.007, 0.014, 0.035 and 0.07 were chosen. These were equivalent to pitch rates of $1^{o}s^{-1}$, $2^{o}s^{-1}$, $5^{o}s^{-1}$ and $10^{o}s^{-1}$ respectively. Static tests were initially performed followed by dynamic tests with the laser and camera in the same position. The digital camera was used for the bulk of the work, and it was used to capture a sequence of images from a single run. In all some 5000 pictures of the flow were taken, which have been archived on CD-ROM. A description of the important results follows.

3.1 Static tests

Figure 6 shows the separated flow over the delta wing at an incidence of 12 degrees. The laser was positioned at the 80% chord location. The right hand portion of the wing is shown, and the wing centre-line is indicated by the white, dashed line to the left of the picture. The wing surface is clearly indicated by the bright, white line running across the image. The significant fluid mechanical features are the primary and secondary vortices. The primary vortex is formed from the roll up of the shear layer separating from the leading edge. Smoke injected at the leading edge infects this shear layer, and hence the primary vortex appears as the anti-clockwise spiral. The secondary vortex is the result of separation induced over the lee surface by the primary vortex (the secondary separation point is clearly seen). Note the well organised structure in the

separated shear layer above and to the left of the secondary vortex. Discrete vortices are often observed in the separated shear layer, and these are the result of a Kelvin-Helmholtz instability. The appearance of the present structure is similar to that reported by Gad-el-Hak & Blackwelder (1985), and further discussion of its behaviour is given in a later section. At lower incidence (see later) the structure is less well defined, and as incidence increases it becomes more energetic. Just inboard of the leading edge, between the shear layer and the wing surface, the fluid recirculates gently.

A sequence of static tests showing the evolution of the flow from low incidence to vortex breakdown is presented in figure 7. Again the laser sheet is at 80% chord, and the wing centre-line is indicated by the white, dashed line. At 5° incidence the vortex is well developed. As incidence increases the vortex strengthens and lifts away from the wing surface and moves slightly inboard. A secondary vortex may just be seen at α=9°. The secondary vortex is almost certainly present below this incidence, and the lack of this feature is probably because no smoke has been entrained into the correct area. However, at 9° the secondary vortex rotates very gently, which indicates that the vortex is very weak or diffuse. Breakdown of the primary vortex sets in at 13° incidence; the core loses its stucture, as shown by the diffusion of the previously clear smoke layers (see section 3.2.4 for more discussion of vortex breakdown). Breakdown first occurs intermittently indicating that the breakdown region oscillates up and down the chord slightly. At 13° the breakdown is permanent, although at 12.5° intermittency is observed. An interesting feature that accompanies instability of the primary vortex is the appearance of a concentrated region of vorticity to the right of the primary vortex. This can be seen in the 12° and 13° cases; it is clear that there is circulation within the structure, owing to the distortion of the smoke around it. Most importantly the structure is not steady. To highlight the unsteadiness figure 8 shows a sequence of pictures, taken 0.2s apart, which show the development and movement of this small vortex. In the first frame the developing vortex A is indicated. In frame (b), 0.2s later, the vortex A has moved to the right and down towards the wing. Meanwhile another vortex B is just starting to develop to the top right of the primary vortex. In frame (c) at 0.4s, the vortex A is now very close to the surface and is positioned to the right of the secondary vortex. Frame (d), at 0.6s, shows that the vortex A has been drawn into the region of slow moving fluid just inboard of the leading edge, and the vortex B is now well defined. The final frame of the sequence (e) at 0.8s shows the vortex B in a more developed state, and an additional vortex C is developing just to the top right of the primary. At this incidence, therefore, the frequency of development of the small vortex structure is approximately 1.3Hz. At 13° incidence, using a conventional video camera and video tape, the frequency is observed to be approximately 2Hz, while at 14° the frequency is more than twice this value.

3.2 Ramp-up tests

For the ramp-up tests the model motion was started at α=0° and stopped at α=35°. With the laser illuminating a given chordwise position runs were recorded at

specified pitch rates. The laser position was then adjusted to the next chordwise position and the camera refocussed as necessary. Each sequence of recorded images was started at a specified incidence, and several sequences for each case were obtained to check for repeatability. To determine the model incidence at each case photographed, the position on the image of the model surface illuminated by the laser sheet was compared with measurements from static cases at known incidences with the camera at the same position and the lens at the same zoom setting. This was not a significant processing burden, since the position of the model surface and the half span width were required anyway. This method of determining incidence was reliable, and did not make any assumptions about the model pitch rate or the camera/ frame grabber framing rate, which would be required if incidence were to be determined simply on the basis of the framing rate, pitch rate and frame number. Once a sequence was recorded the images were immediately available for analysis. A description of the evolution of the flow with incidence and chordwise position for a number of pitch rates follows.

3.2.1 Development of flow patterns at 80% chord

The following descriptions of the flow patterns and the figures accompanying them are typical of the runs performed.

Figure 9 shows a sequence of images for a reduced pitch rate of 0.007 ($1^o s^{-1}$) at the 80% chord location. At 5° the primary vortex is well formed, and its appearance is not much different from the static case at the same incidence (figure 7a). As the model pitches to higher incidence the appearance of the primary vortex does not differ appreciably from the static case at all; frame 9e at 12° even shows evidence of the small, unsteady vortex structure described in figure 8. However, at 13° the flow pattern is clearly different from the static case; the pitching case shows a distinct vortex core, as defined by the clear smoke layers, while the static case (figure 7f) shows that the core has burst. Note however, that in the pitching case the outer smoke layers of the vortex, to the lower left of the primary core, are significantly distorted. At 14° , figure 9g, the smoke layers in the vortex core are distorted, although they are still distinct. At 15°, figure 9h, all structure within the core has disappeared, and the core may be judged to have burst. This final burst is at an incidence some 2.5° higher than in the static case.

A sequence of images for a reduced pitch rate of 0.014 ($2^o s^{-1}$) is shown in figure 10. Frame (a) is at an icidence of 5.4°. There are no significant structural differences compared to the case at 1^o s^{-1} (figure 9a), although examination of the full scale image from which this figure was derived suggests that the vortex spiral has fewer turns in the higher pitch rate case. This suggests a lower vortex strength, although it may also be a result of the smaller non-dimensional times. No other significant structural differences are noted until 14° is reached. In the k=0.007 case the centre of the vortex becomes distorted, while in the present case the definition within the centre remains good. The outer layers to the lower left of the vortex core are significantly distorted, however. This pattern remains as incidence increases further; frame (i) at 15.6° shows that the vortex has distorted

to an elliptical shape with significant distortion in the outer layers of the vortex. Frame (j) at 16.4° indicates that any structure within the vortex core has all but disappeared; the vortex has burst some 4° higher than in the static case.

The final sequence of images, figure 11, at this chordwise position is for a reduced pitch rate of 0.035 ($5°s^{-1}$). The 5° case (figure 11a) shows that the primary vortex has barely developed and that it is very close to the leading edge compared to the lower pitch rate cases (figures 10a and 9a). The next frame at 7° shows that the vortex core is more fully developed; comparison with the static case (figure 7b) shows a noticeably lower number of turns in the spiral caused by the primary vortex. Again this could be due to the effects of lower non-dimensional times (at this pitch rate one chord length of travel corresponds to 4° of pitching motion) and/ or lower vortex strength. Apart from the inboard and upward vortex movement, no other significant structural differences are noted until the model reaches 14° incidence. At this incidence, figure 11g shows that the smoke layers within the centre of the vortex are just beginning to distort. Note also the waviness in the shear layer prior to its roll up into the primary vortex; this is evidence of instability in the shear layer. 1° later at 15°, figure 11h shows that the distortion has grown radially outwards to affect more of the vortex core. At 16° the disturbance has progressed further, and the vortex appears to have been squashed. There is also some distortion of the outer layers of the vortex above the vortex core. At 17°, figure 11j, the vortex has been further flattened. The vortex core, although having lost its internal structure, is still relatively compact. Figures 11k and 11l at 18° and 19° show the further distortion of the primary vortex.

3.2.2 Development of flow patterns at 40% chord

For comparison with the dynamic tests a sequence of static tests from the 40% chord location is shown in figure 12. No significant behavioural differences were observed in the static tests further up the wing except for the appearance of the periodic vortex structure described in figure8; at the more forward locations this structure was not visible, indicating that the vortex was the result of the downstream growth of a disturbance.

Figure 13 shows the ramp-up case at a reduced pitch rate of 0.007 ($1°s^{-1}$). The vortex development is similar to the x/c=0.8 case, except that the vortex does not break down until a significantly higher incidence. In this case the first distortion seen in the vortex centre is at 18° (figure 13g) and at 19° the structure of the core has disappeared. Vortex burst is some 1° later than in the static case.

The test at k=0.014 ($2°s^{-1}$), figure 14, again reveals features similar to the more downstream location described in section 3.2.1. The outer layers of the vortex first show distortion at 18.6° (figure 14g). This distortion grows as incidence increases, although the structure of the smoke layers within the centre of the vortex remains clear until α=21° (figure 14j).

At k=0.035 ($5^o s^{-1}$), figure 15, similar behaviour to above is observed. Distortion of the vortex is first observed at 19°, figure 15e, where the smoke on the outside of the vortex to the left of the vortex core has developed a sharp kink. The outer layers of the vortex then become more and more distorted as incidence increases; figure 15f at 20° suggests that these distortions are in fact discrete vortex structures. Up until 24°, figure 15j, however, the centre of the vortex remains distinct and clear and the vortex core remains tight. At 25°, figure 15k, the smoke structure at the vortex centre has gone.

3.2.3 Vortex position measurements

From the images the spanwise position and height of the primary vortex may be measured easily. Figure 16 shows the variation of vortex position with incidence as a function of chordwise position at a number of reduced pitch rates. The spanwise position is measured from the wing centre-line, and both vortex height from the wing surface and spanwise position are non-dimensionalized with respect to wing local semi-span.

Figure 16a is for the static case. As incidence increases the vortex moves initially inboard and away from the wing surface for all chordwise locations. At x/c=0.9, the vortex suddenly moves outboard just prior to burst (α=11°). Indeed, for all the chordwise positions the vortex moves outboard before vortex burst; at x/c=0.7, the outboard movement starts at α=11°, and at x/c=0.5 and x/c=0.3 it starts at α=12°. The vortex is marginally more inboard closer to the trailing edge, and is displaced further from the wing surface at the more forward locations. Once burst has crossed the trailing edge then the spanwise position of the vortex may vary more along the model chord.

At the reduced pitch rate of 0.007, figure 16b, similar observations to the static case are made. As incidence increases the vortex moves inboard and away from the wing, and the vortex is marginally more inboard and noticeably further from the wing surface at the more forward locations. Again, the outboard movement prior to burst starts at lower incidence towards the trailing edge.

The above behaviour is again observed at the k=0.014 case (figure 16c). However, at the higher pitch rates (k=0.035 and k=0.07, figures 16d and 16e respectively) the initial vortex formation is much further outboard at the more aft locations, and the variation in vortex displacement from the wing surface with chordwise location is not so strong. At these pitch rates the more outboard vortex formation at the more aft locations is probably due to the greater distance from the pitch axis; the effect will be similar to that of the flow observed behind an impulsively started flat plate, with the impulse velocity of greater value at the more aft locations. Note also in the k=0.07 case that the vortex does not move back outboard prior to vortex burst.

Figures 17a-d show the same data as above, except that the vortex position is presented as a function of pitch rate at various chordwise locations. The figures show that for a given incidence the vortex is generally further outboard and

closer to the wing in the higher pitch rate cases. This behaviour would be expected from the impulsively started plate analogy. Note also that the rate of vortex inboard movement with incidence prior to breakdown is essentially the same for all the pitch rates shown.

3.2.4 Vortex burst measurements

Vortex burst is associated with an abrupt deceleration of the fluid in the vortex core; as a consequence of this the vortex core diverges rapidly. The latter observation may be used to interpret vortex burst from the present visualization tests. Using the present visualization, therefore, in the static tests vortex burst was accompanied by the rapid disappearance of the tight, uniformly-wound, spiral pattern of the smoke; this loss of structure was first manifested by a radially outward growth of a disturbance from the centre of the vortex, indicative of a sudden expansion of the vortex core. Assuming a similar physical mechanism of vortex burst in the pitching case, then a smoke pattern compatible with that of burst in the static case may be expected; this would provide a basis for measurement of vortex burst incidence in the pitching case. However, as described in section 3.2 above, in the dynamic case significant vortex distortion was often observed well before loss of structure within the centre of the vortex itself. This is particularly well illustrated in figure 18, which shows a sequence of images revealing the vortex bursting at the 80% chord location at a reduced pitch rate of k=0.014 ($2^{o}s^{-1}$). Figure 18a, at 11.6°, shows a 'folded' smoke layer to the left of the vortex centre (this is indicated). This becomes clearer in the next frames at 12° and 12.4°. Frame (d) at 13° shows no significant distortion. However frame (e) at 13.4° shows significant folding of the smoke layers to the lower left of the vortex centre. In the next frame, at 13.8°, this distortion has become greater, and other folds appear elsewhere. At 14.2° in addition to the folding of the smoke layers, the vortex has lost its nominally circular shape and is flattened into a more elliptical shape. Frame (h) at 14° shows a further development of this pattern, while frame (i) at 15° shows a further re-orientation of the vortex. Note, however, that in spite of this gross distortion of the vortex, a distinct, clear vortex centre remains. The next frame at 15.4° shows the first sign of a disturbance at the vortex centre itself. The smoke layers are still distinct, although there is a great degree of folding there. Frame (k), at 15.8°, shows the almost complete loss of any structure within the vortex core. It would appear, therefore, that once any disturbance appears at the vortex centre, its rate of growth is enormous compared with disturbances observed elsewhere.

The above pattern of events was observed in the majority of cases. The appearance of the distortion of the vortex seen in the outer smoke layers (the folding) is compatible with a localized roll up of the feeding shear layer; Lowson (1991) observed similar features which were associated with a transition to turbulence in the shear layer. For the present purposes, therefore, vortex burst is defined visually as the complete loss of any structure within the vortex core. Note that this loss of structure at the vortex centre accompanies an expansion of the core. From figure 18, therefore, frame (k) at 15.8° may be said to show a burst vortex. Frame (j) at 15.4° shows the beginning of vortex burst. The appearance of vortex burst itself as the momentary folding of the smoke layers in the vortex

centre followed rapidly by a complete destruction of the distinct smoke layers suggests a growth of flow structures from a large to a small scale, and therefore a development of a disturbance from a low frequency to a high frequency.

From the images an attempt has been made to measure vortex burst incidences. Note that there is a degree of subjectivity in the visual interpretation of vortex breakdown. The primary visual signal was the disappearance of well defined structure from the centre of the vortex. However, the visual definition in the pitching case needed to be compatible with that in the non-pitching case. In the non-pitching case the onset of burst at a given chordwise location was seen to be intermittent; this intermittency had more or less completely disappeared when the burst smoke pattern had filled approximately half of the cross sectional area of the vortex (e.g. figure 7f). This 'degree' of burst was therefore used as a benchmark for determination of burst incidence at a given chordwise location; sample figures showing dynamic burst are figures 9h, 10j, 11j, 13h, 14j and 15k. Data showing burst progression up the wing are plotted in figure 19a for the static case and dynamic cases at k=0.007, 0.014, 0.035 and 0.07 in the range $0.4<x/c<0.9$. In each case burst proceeds uniformly from the trailing edge to the apex as incidence increases, and for a given chordwise location burst occurs at a higher incidence the higher the pitch rate. The average velocity of burst progression is shown in figure 19b; as pitch rate increases, burst progresses up the wing at a faster rate. Note, however, that the burst velocity does not increase linearly with the reduced pitch rate. If this were the case, then the rate of progression of burst up the wing with incidence would be the same for each pitch rate, which is clearly not the case on figure 19a. There are therefore two factors that delay the progression of burst up the wing, both of which appear to depend upon the pitch rate. These are a delay in the onset of burst at the trailing edge and an additional delay in its progression up the wing.

3.3 Ramp-down tests

The procedure for the ramp-down tests was essentially identical to that of the ramp-up tests, except that the model motion started at 30° and finished at -5°. The main focus of the ramp-down tests was to determine the vortex 'restoration' incidence and the vortex behaviour following restoration. Note that the term restoration here is simply meant to indicate the return to non-burst behaviour.

3.3.1 Development of flow pattern during ramp-down test

A typical sequence of images from a ramp-down test is shown in figure 20. In this figure the x/c=0.8 position is illuminated and the reduced pitch rate is k=-0.035. Quite clearly frame (a) at 8° shows a broken down vortex; this case is some 4.5° below the nominal static breakdown incidence. At a sufficiently low incidence the vortex begins to reform; figure 20b at 5° shows that the outer layer of the vortex has become well defined. As incidence decreases further the region of poor smoke definition becomes confined to a smaller and smaller area around the vortex centre, until at 2°, frame (e), the vortex regains its well-defined, spiral appearance. Note that in a static test the vortex was not discernible at this incidence. As the wing continues to pitch down the vortex weakens and

eventually disappears; at this high pitch rate the vortex is still present at α=-3°, however. After vortex restoration during a ramp-down test the smoke pattern shows none of the folding seen prior to vortex burst in the ramp-up test. This is presumably because of the much lower incidence at which the vortex reforms compared to the high incidences experienced prior to burst in the pitch-up case.

3.3.2 Vortex position measurements

Vortex position after vortex restoration was measured in the same way as for vortex position prior to burst in the ramp-up tests. Figure 21 shows the variation of vortex position over the wing with incidence during pitch-down motion as a function of chordwise location at a number of pitch rates. Figure 21a, at k=-0.035, shows that after vortex restoration the vortex moves noticeably inboard at x/c=0.7 and x/c=0.9, while at the x/c=0.5 location the vortex remains at a nominally constant spanwise position. In all cases the vortex moves closer to the wing surface as the wing pitches down. At k=-0.014, figure 21b shows similar behaviour to the k=-0.035 case, except that at the x/c=0.7 and 0.9 positions the vortex does not start to move inboard until the wing reaches an incidence of approximately 3°. Finally figure 21c for k=-0.007 shows that after vortex restoration the vortex moves slightly inboard and then outboard as the wing pitches down, although below 2° the aft locations show that the vortex suddenly moves inboard.

An alternative presentation of the above data is given in figure 22, where the effect of pitch rate is shown for a given chordwise position. As remarked above the effect of pitch rate is significant at the x/c=0.9 and 0.7 locations, in that the spanwise position of the vortex changes with decreasing incidence in a different manner for each pitch rate. At x/c=0.5, the vortex is much further inboard for the highest pitch rate test, although the vortex remains relatively stationary as the wing pitches down.

3.3.3 Vortex restoration measurements

During the ramp-down test the vortex starts from the fully broken down state. If the model pitches to low enough incidence the vortex will eventually reform to form the well-defined, tightly wound structure associated with the unburst vortex. Rather than define a degree of burst as for the pitch up case, in the pitch down case the primary vortex may be viewed to have reformed when all distortion at the vortex centre has disappeared; thus figure 20e shows the first indication of a fully reformed vortex during ramp-down motion. This definition is not consistent with that used for ramp-up motion, although in that case the vortex was bursting.

Vortex restoration incidences were measured at a number of chordwise locations and pitch rates, and figure 23a shows the effect of pitch rate upon vortex restoration incidence. The data shown are averages of four tests. Note that the static data refer to vortex burst. In all cases the vortex restoration during ramp-down motion occurs below the static burst incidence, and the greater the pitch rate the greater is the extension of burst vortex behaviour to low incidence. For

each pitch rate restoration progresses steadily along the wing from the apex to the trailing edge. The rate of progression with incidence shows a weak decrease with increasing pitch rate, which means that the restoration velocity increases with reduced pitch rate. Figure 23b shows the non-dimensional restoration velocity as a function of reduced pitch rate. Therefore, there are two factors that delay vortex restoration, both of which depend upon the pitch rate; a delay in the onset of restoration at the apex and a delay in its subsequent progression along the chord.

4. Discussion

A flow visualization study of a pitching delta wing has been performed. Detailed photographic sequences showing flow development, and results describing vortex position, vortex breakdown and vortex restoration during constant pitch rate pitch-up and pitch-down motions have been presented.

It is well known that the aerodynamic coefficients for a pitching delta wing differ considerably from the static case at the same incidence (e.g. Ashley et al. (1991), Huyer et al. (1992)). Although much of this effect is due to lag in the vortex development, some of the effect is due to vortex position. In extreme cases, the present results have shown that the primary vortex structure may be very far outboard compared to the static case in the pitch-up case. Therefore in addition to control problems, this has implications for the interaction of the vortex structures with other lifting and control surfaces.

The most important feature of the delta wing flow that limits the performance of the wing is vortex breakdown, however. In the present case, vortex breakdown has been measured during static tests and pitch-up and vortex 'restoration' has been measured during pitch-down. In any presentation of vortex burst measurements it is essential to draw comparison with any other available data. For this purpose the papers by Wolffelt (1986), Miau et al. (1992) and Lowson & Riley (1995) may be referred to. Lowson & Riley (1995) compiled vortex breakdown incidences measured by a number of investigators; for the 60° sweep wing the trailing edge breakdown incidence recorded by the various investigators ranged from 9° to 16°, and Lowson & Riley's main conclusion was that wing and apex geometry had the most significant effect upon vortex burst location. Miau et al. (1992) have performed tests on a 59° sweep delta over a range of pitch rates at Reynolds numbers comparable to the present tests. It is noted that the static test burst incidences during the present tests are some 3° earlier than in Miau et als' results. This difference between the current results and Miau et als' results is well within the range of results reported by Lowson & Riley, and in the light of Lowson & Riley' s investigation, the difference is not surprising, since Miau et als' delta wing was essentially a 1mm thick, square-cut flat plate, whereas the present model geometry is considerably different. In spite of this difference in burst incidence, the rate of progression of burst up the wing is essentially the same in the two sets of tests.

Differences in detailed behaviour between the current data and Miau et als' data are noted when the pitching data are compared. The most significant difference in the pitch-up behaviour is revealed as pitch rate increases. Miau et als' data

show that for x/c<0.7 breakdown occurs earlier for the k=0.02 case than for the k=0.01 case, and they also comment that the propagation rate of breakdown is proportional to the pitch rate (in the present tests, breakdown took relatively longer, in terms of incidence range, to proceed up the wing as pitch rate increases). Most significantly, however, for k=0.04 they observe a brief deceleration or 'plateau' in the breakdown progression up the wing (for convenience Miau et als' k=0.04 data are plotted on figure 19). At this pitch rate breakdown was observed to proceed uniformly up the wing to the 60% chord region; it then did not progress significantly beyond this point for another 4º of pitch, after which it proceeded uniformly up the wing at approximately the same rate as before the plateau. This feature is absent from the present data. Even when tests were performed starting from the pitch angle where burst was just about to cross the trailing edge (as in Miau et als' tests), the plateau was not observed. Miau et al. could not definitely attribute the presence of their plateau to any particular physical phenomenon, although it was suggested that the secondary vortex formation played a role. The work by Wolffelt (1986) was limited to one pitch rate, and investigated the effect of changing the start incidence. No plateau similar to Miau et al. was observed.

In view of the above described discrepancies in burst behaviour during pitch up, attention must be payed to the rigourousness and accuracy of the current tests. For the purposes of determining the breakdown incidence the laser sheet was positioned at the required chordwise position with the model at the expected incidence, and the camera was focussed upon this location. Therefore, there is very little error in the measurement of the chordwise location itself. Using the photographic calibration method, the incidence measurement is accurate to better than 0.25º. In the author's opinion, the only significant error in the determination of burst incidence is in the subjectivity involved in the interpretation of burst. The criteria described in section 3.2.4 were used when defining burst; there is no scope within the confidence limits of the present analysis to accomodate a plateau similar to that observed by Miau et al.

In the pitch up case, therefore, the present results indicate that the delay in vortex burst consists of a delay in the passage of burst over the trailing edge and a further delay in the progression of burst up the wing. Both of these effects are pitch rate dependent. Note that both the present results and those of Miau et al do not find agreement with Rediniotis et als' (1994) conclusion that burst appeared almost simultaneously along the entire chord of the wing during dynamic pitch up. Their conclusion was based upon their low incidence resolution, and in view of this they suggested that breakdown propagates with great speed. The present results indicate that even though propagation of breakdown may be fast in terms of velocity at the high pitch rate, it still requires a large, finite incidence change to progress up the wing

An interesting and useful observation from the sequences of images depicting vortex burst in the pitching case is that the visual appearance of burst in the pitching case is essentially the same as in the static case. Burst first appears as the folding of the smoke layers at the vortex centre, rapidly followed by the radially outward growth of the disturbed region of smoke. This indicates that the physical

mechanism of burst is the same in the static and pitching cases, which may be contrasted with stall over 2-D aerofoils, where the flow physics in the pitching case differ greatly from the steady case. However in the pitching case burst is 'stretched' over a range of incidences, and there may be significant distortion of the vortex core before burst itself (e.g. figure 18). While in the static case a 0.5° increase in incidence is enough to cause a complete transition from the unburst/ intermittent burst behaviour to fully burst behaviour, a 1° incidence increase in the k=0.007 case (figures 9g and 9h) and a 3° increase in the k=0.035 case (figures 11g to 11j) reveal the transition. These incidence increases correspond to non-dimensional times of the order of 1.0, and this time reflects the time required for growth of the disturbances associated with vortex burst.

Detail of the behaviour of the vortex centre during the development of vortex burst is shown in figure 24. Frame (a) at 14° shows the first folding of the smoke filamants at the vortex centre. One degree, or 0.2s later, at 15° the extent of the development of this disturbance is clearly seen; the smoke pattern is compatible with what may be observed if the vortex core was splitting into a number of smaller structures. Frame (c) at 16° shows the further development, indicating again that the development of burst in the present case may be associated with a splitting up of the primary vortex core. Parker (1977) suggested that the mode of burst changed in unsteady flow. In the present case the core breaks down into a diffuse region, while in many of the dynamic cases some powerful structures were observed before the final breakdown into fine scale turbulence. This reflects Parker's observations. Further discussion of the physics of vortex burst from the present flow visualization is difficult without quantitative information in three dimensions, and this is the subject of further effort. Detailed computations (Visbal (1994)) have identified the details of the cross-flow topological changes during vortex burst, and other PIV studies (Lin & Rockwell (1995)) have identified the generation of azimuthal vortices during burst. Future work will extend these studies by quantifying the re-distribution of axial vorticity during pitching motion.

5. Conclusions

A detailed flow visualization of a 60° sweep, pitching delta wing has been performed. During pitch up motions the vortex is further outboard and closer to the wing surface than in the non-pitching case. Vortex burst is delayed, and the delay is dependent upon the pitch rate. Burst progresses at a uniform rate up the wing, and the speed of progression of burst up the wing increases with pitch rate. The visual appearance of burst is the same in the pitching and non-pitching cases, and appears as a rapid distortion of the smoke lines at the vortex centre which grows radially outwards. During pitch down motion of the wing well defined, coherent vortex motion is not observed until well below the non-pitching burst incidence, and the degree of delay increases with pitch rate. At high enough pitch rate a significant vortex may be observed at negative incidence.

6. Acknowledgements

Financial assistance for the present work was obtained from the Nuffield Foundation, the Royal Society and the John Robertson and Dunlop Chapman bequests of the University of Glasgow. The assistance of Mr. M.L. Jupp and Dr. F.N. Coton during the progress of this work is acknowledged.

7. References

Ashley, H., Katz, J., Jarrah, M.A., & Vaneck, T. (1991) 'Survey of Research on Unsteady Aerodynamic Loading of Delta Wings' J. Fluids & Struct., 5, pp 363-390

Cornelius, K.C. (1995) 'Analysis of vortex bursting using three-dimensional laser measurements' J. Aircraft, 32, pp 297-306

Erickson, G.E. (1995) 'High angle of attack aerodynamics' Ann. Rev. Fluid Mech. 27, pp 48-88

Gad-el-Hak, M. & Blackwelder, R.F. (1985) 'The Discrete Vortices from a Delta Wing' A.I.A.A. J., 23, pp 961-962

Greenwell, D.I. & Wood, N.J. (1992) 'Determination of vortex burst location on delta wings from surface pressure measurements' A.I.A.A. J. 30, pp 2736-2739

Gursul, I. & Yang, H. (1995) 'Vortex Breakdown over a Pitching Delta Wing' J. Fluids & Struct, 9, pp 571-583

Harvey, J.K. (1960) 'Some observations of the vortex breakdown phenomenon' J. Fluid Mech., 14, pp 585-592

Honkan, A. & Andreopoulos, J. (1997) 'Instantaneous Three-Dimensional Vorticity Measurements in Vortical Flow over a Delta Wing' A.I.A.A. J., 35, pp 1612-1620

Hudson, L.J., King, P.I. & David, M. (1989) 'Flow separation and vortex locations on wings pitching at constant rates' A.I.A.A.-89-2160-CP, Atmospheric Flight Mechanics Conference, Minneapolis, U.S.A.

Huyer, S.A., Robinson, M.C. & Luttges, M.W. (1992) 'Unsteady Aerodynamic Loading Produced by a Sinusoidally Oscillating Delta Wing' J. Aircraft, 29, pp 366-373

Jupp, M.L., Coton, F.N. & Green, R.B. (1998) 'A Statistical Analysis of Surface Pressure Measurements With Particular Reference to Vortex Breakdown' University of Glasgow, Department of Aerospace Engineering, G.U. Aero Report 9806, Glasgow, Scotland.

LeMay, S.P., Batill, S.M., Nelson, R.C. (1990) 'Vortex Dynamics on a Pitching Delta Wing' J. Aircraft, 27, pp 131-138

Lin, J.-C. & Rockwell, D.O. (1995) 'Transient structure of vortex breakdown on a delta wing' AIAA Journal, 33, pp 6-12

Lowson, M.V. (1991) 'Visualization Measurements of Vortex Flows' J. Aircraft, 28, pp 320-327

Lowson, M.V. & Riley, A.J. (1995) 'Vortex Breakdown Control by Delta Wing Geometry' J. Aircraft, 32, pp 832-838

Magness, C., Robinson, O. & Rockwell, D. (1993) 'Instantaneous Topology Showing the Unsteady Leading Edge Vortex at High Angle of Attack' A.I.A.A. J., 31, pp 1384-1391

Miau, J.J., Chang, R.C., Chou, J.H. & Lin, C.K. (1992) 'Nonuniform Motion of Leading-Edge Vortex Breakdown on Ramp Pitching Delta Wings' A.I.A.A. J., 30, pp 1691-1702

Parker, A.G. (1977) 'Measurements on a Delta Wing in Unsteady Flow' J. Aircraft, 14, pp 547-552

Rediniotis, O.K., Klute, S.M., Hoang, N.T. & Telionis, D.P. (1994) 'Dynamic Pitch-Up of a Delta Wing' A.I.A.A. Journal, 32, pp 716-725

Vaughan, J.P. & Wood, N.J. (1995) 'Pressure measurements on a half delta wing oscilalting in pitch' Aero. J. 99, pp 432-438

Visbal, M.R. (1994) 'Onset of Vortex Breakdown Above a Pitching Delta Wing' A.I.A.A. J., 32, pp 1568-1575

Wolffelt, K.W. (1986) 'Investigation of the movement of vortex burst position with dynamically changing angle of attack for a schematic delta wing in water tunnel with correlation to similar studies in a wind tunnel.' AGARD CP-413

8. Figures

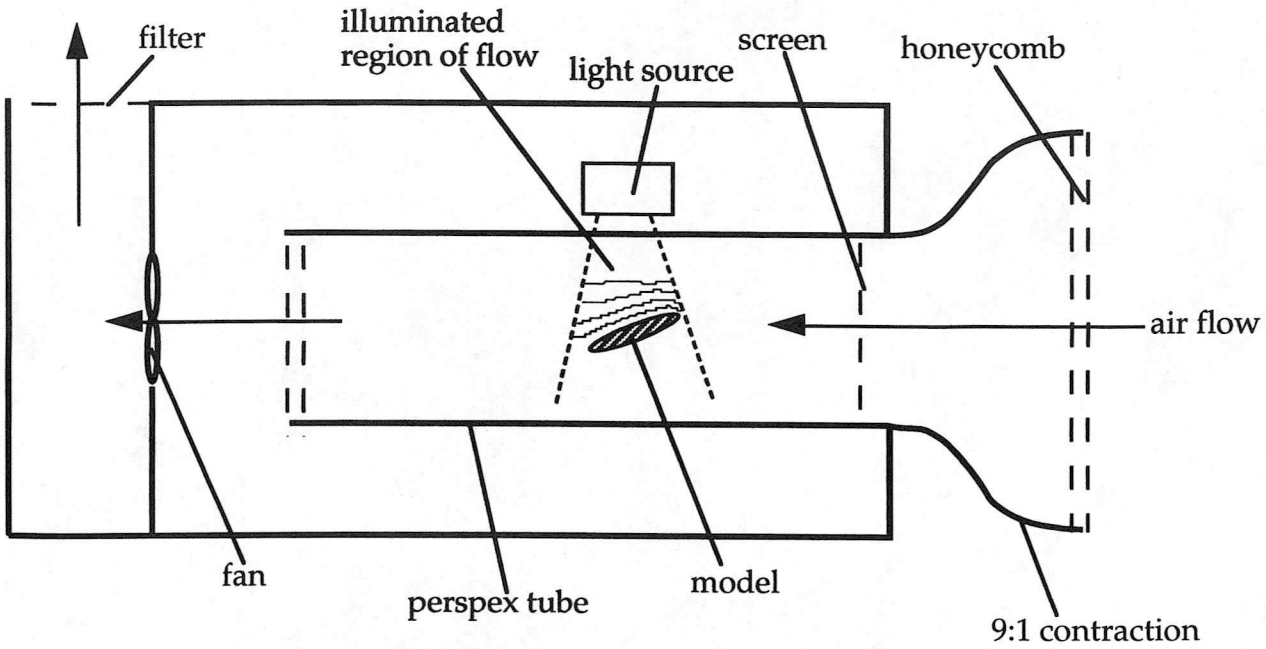

Figure 1 Schematic diagram of smoke flow visualization wind tunnel

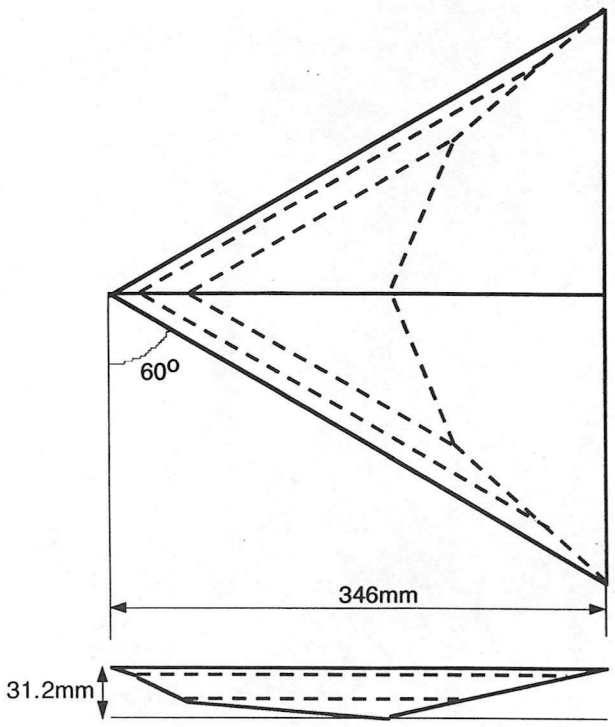

Figure 2 Scale drawing of the delta wing used in the tests.

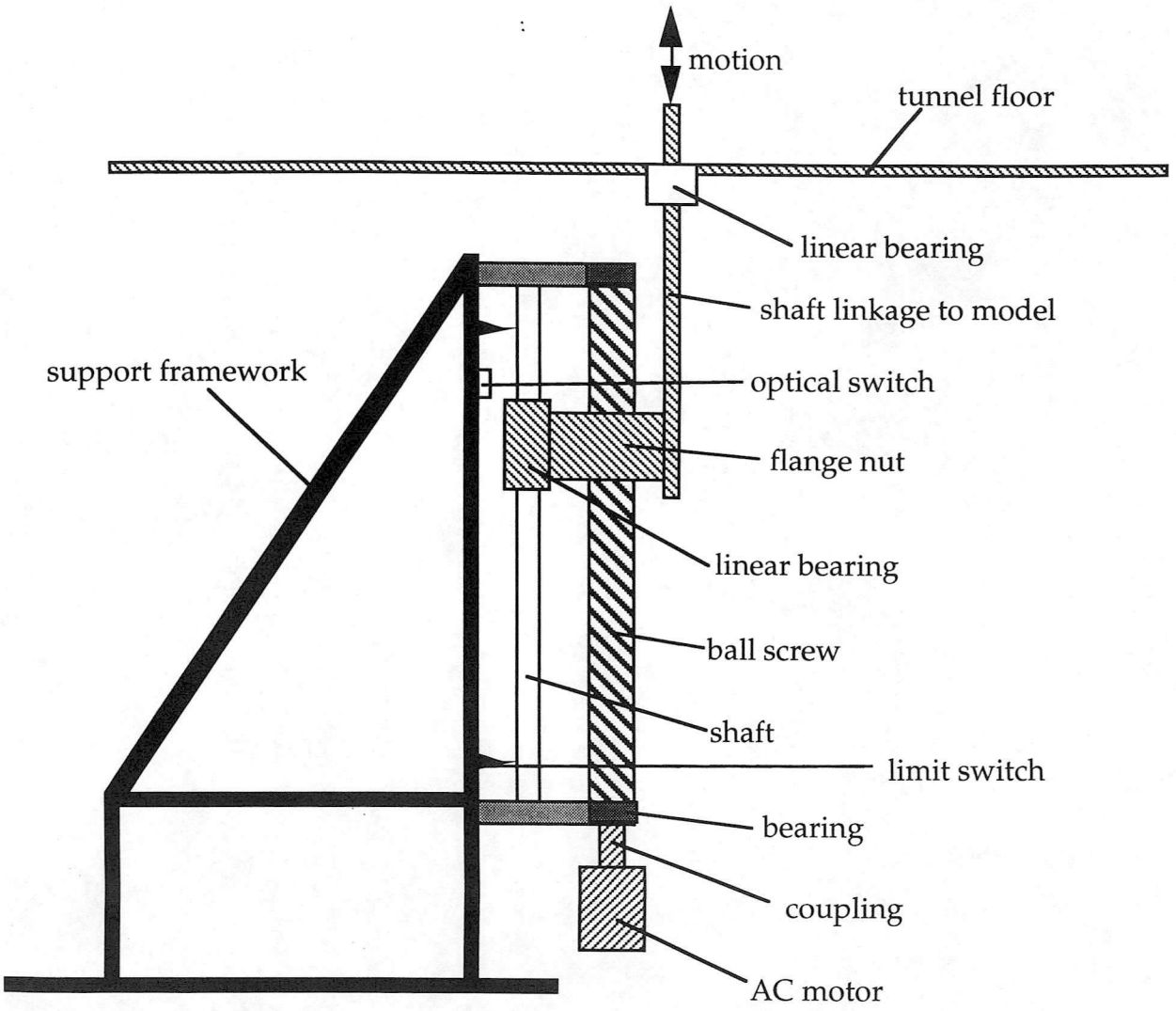

Figure 3 Schematic of model actuation apparatus

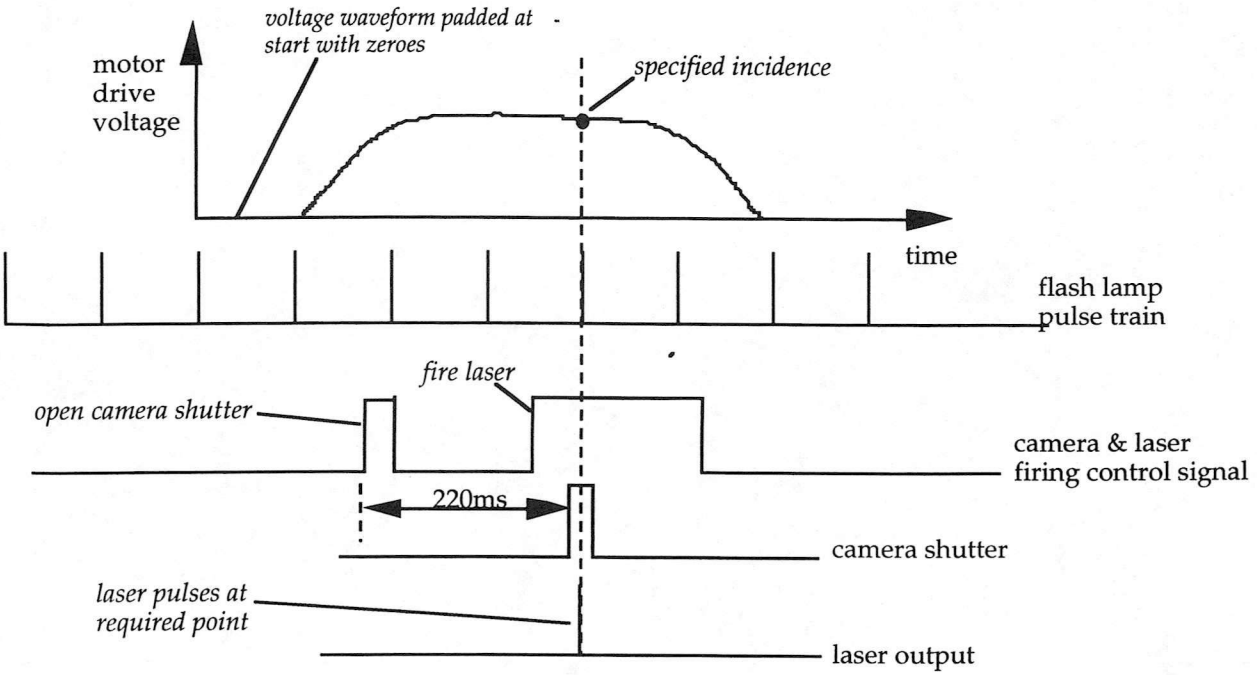

laser pulse is synchronized with model motion by synchronizing drive voltage generation with flash lamp pulses and padding the start of the drive voltage signal with zeroes. Note laser fire signal comes before the desired flash lamp pulse.

Figure 4 Synchronization of Nd:YAG laser with model motion.

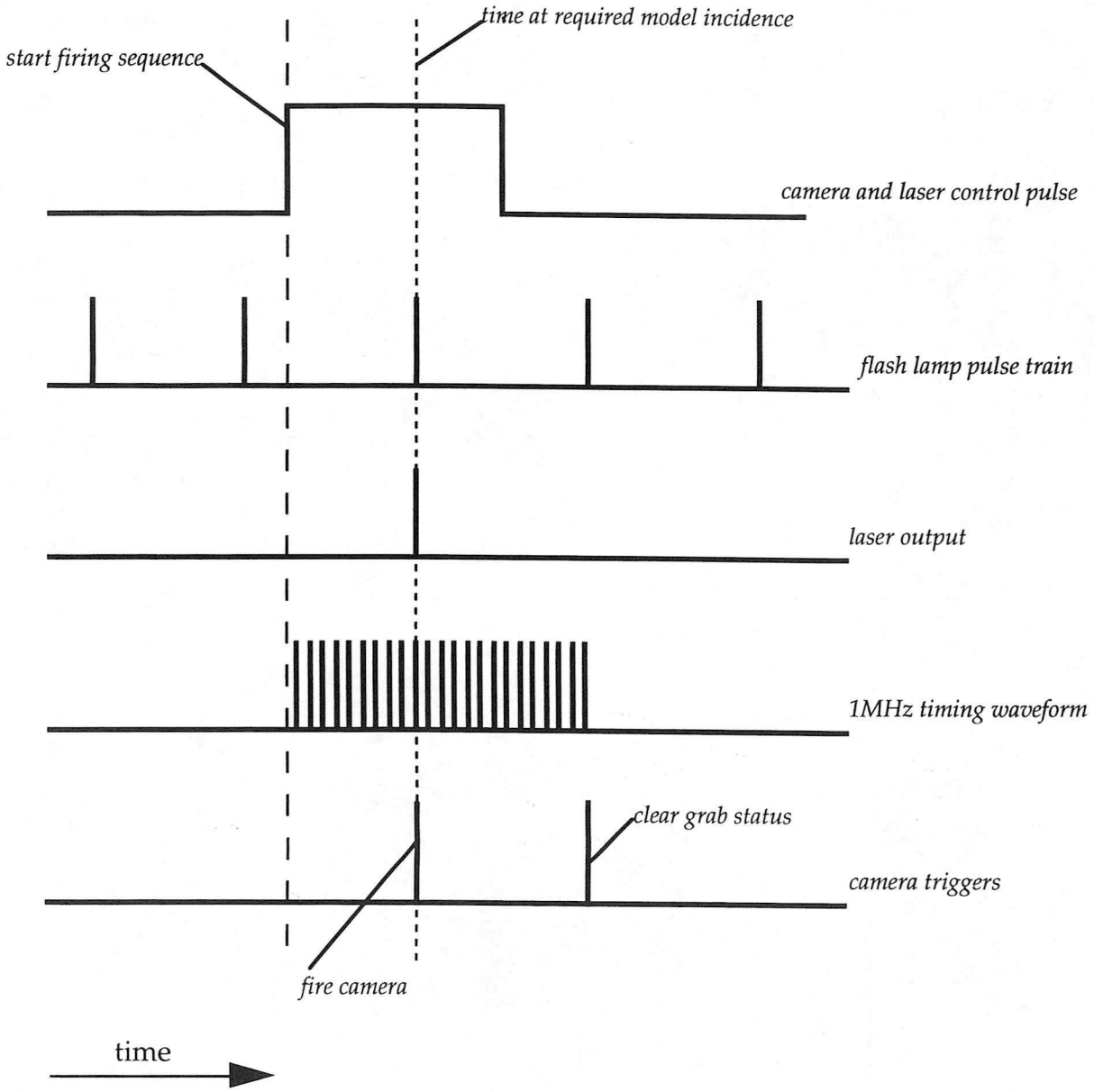

Figure 5 Timing diagram for triggering the digital video camera

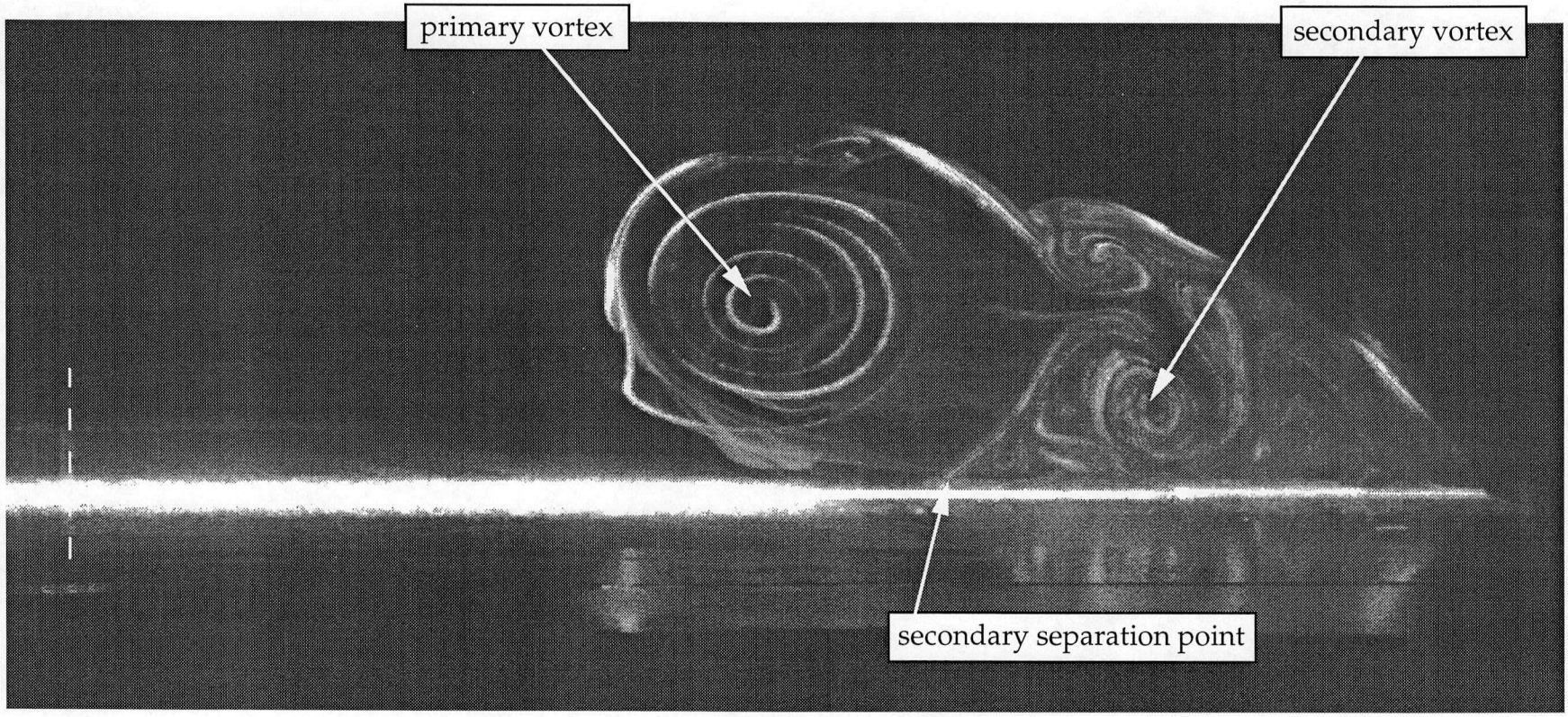

Figure 6 Vortex system over the delta wing at 12 degrees incidence. Laser sheet at 80% chord position. Nominal Reynolds number = 10000. The position of the wing centre-line is indicated by the white, dashed line. The salient features are indicated.

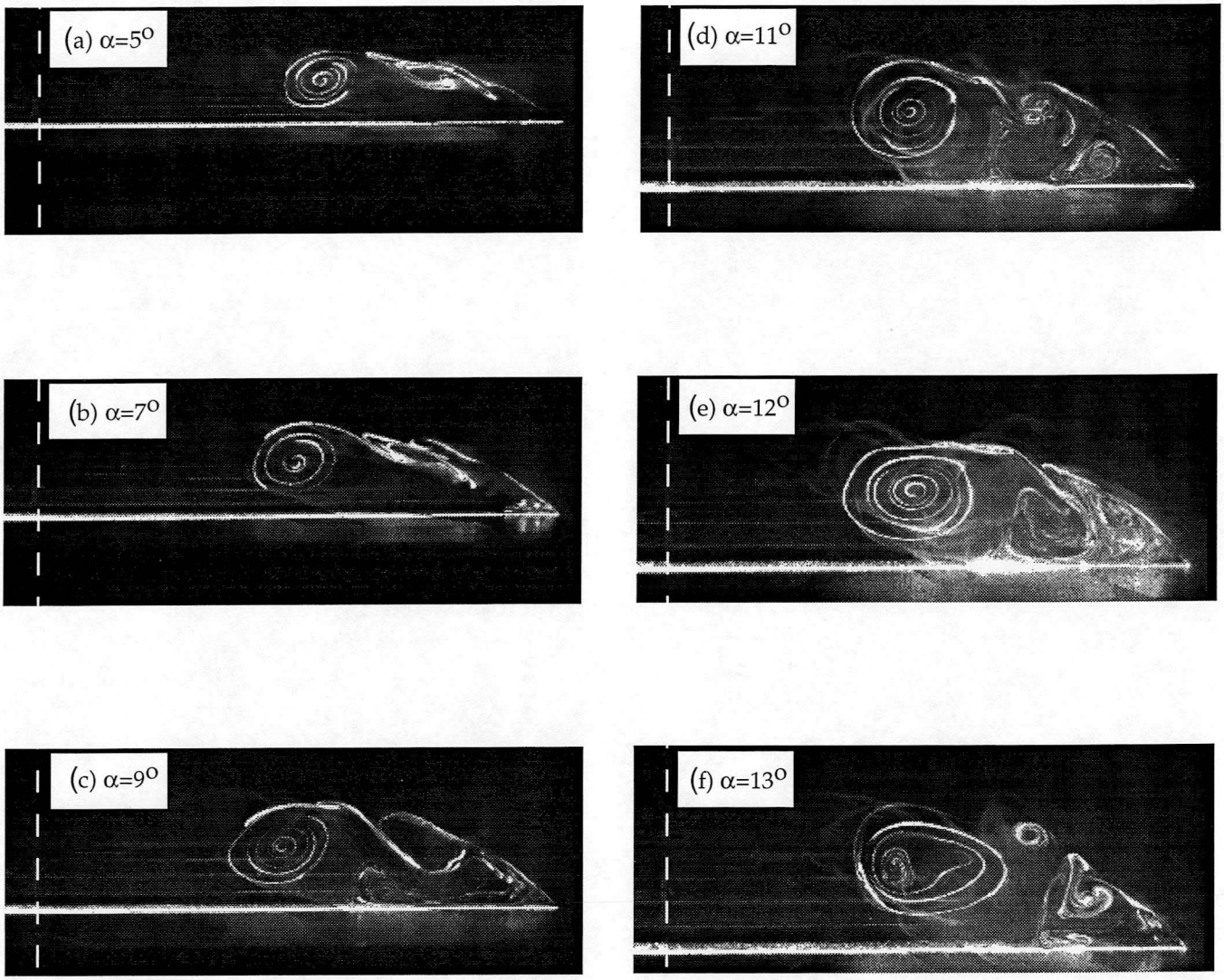

Figure 7 Flow visualization at fixed incidence at x/c=0.8. The model incidence is indicated on each picture

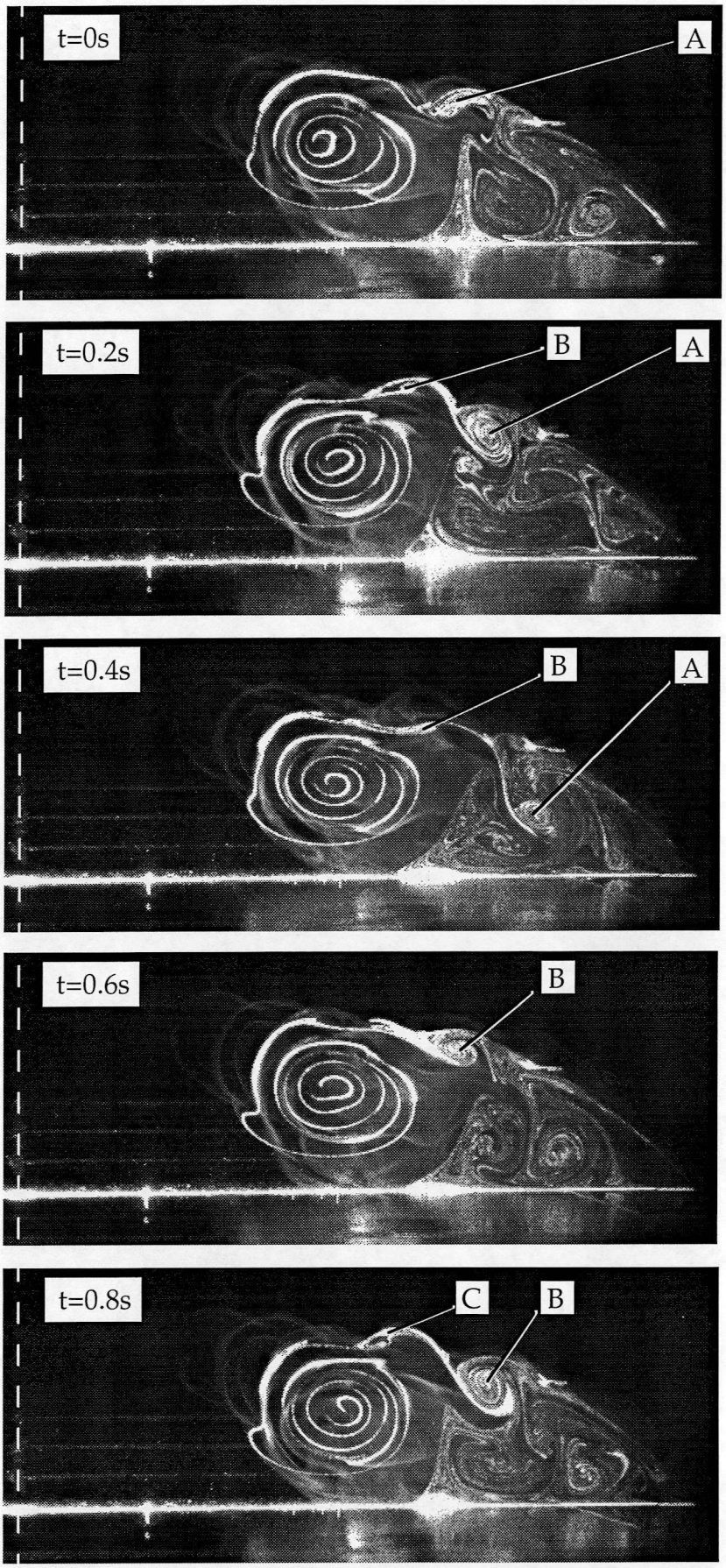

Figure 8 Sequence of images separated by 0.2s at $\alpha=12^{o}$, x/c=0.8. Note the development of the unsteady flow features indicated A, B and C.

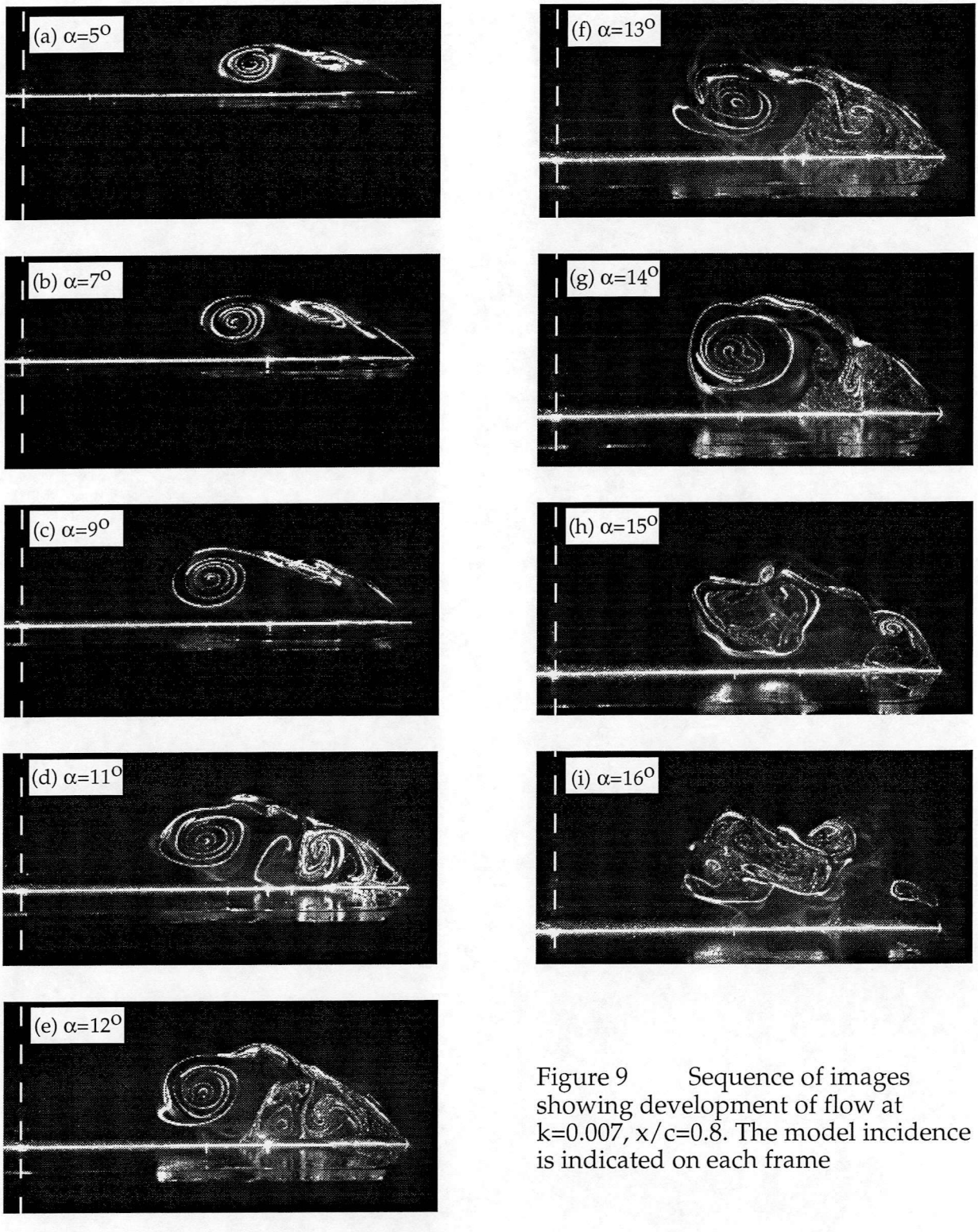

Figure 9 Sequence of images showing development of flow at k=0.007, x/c=0.8. The model incidence is indicated on each frame

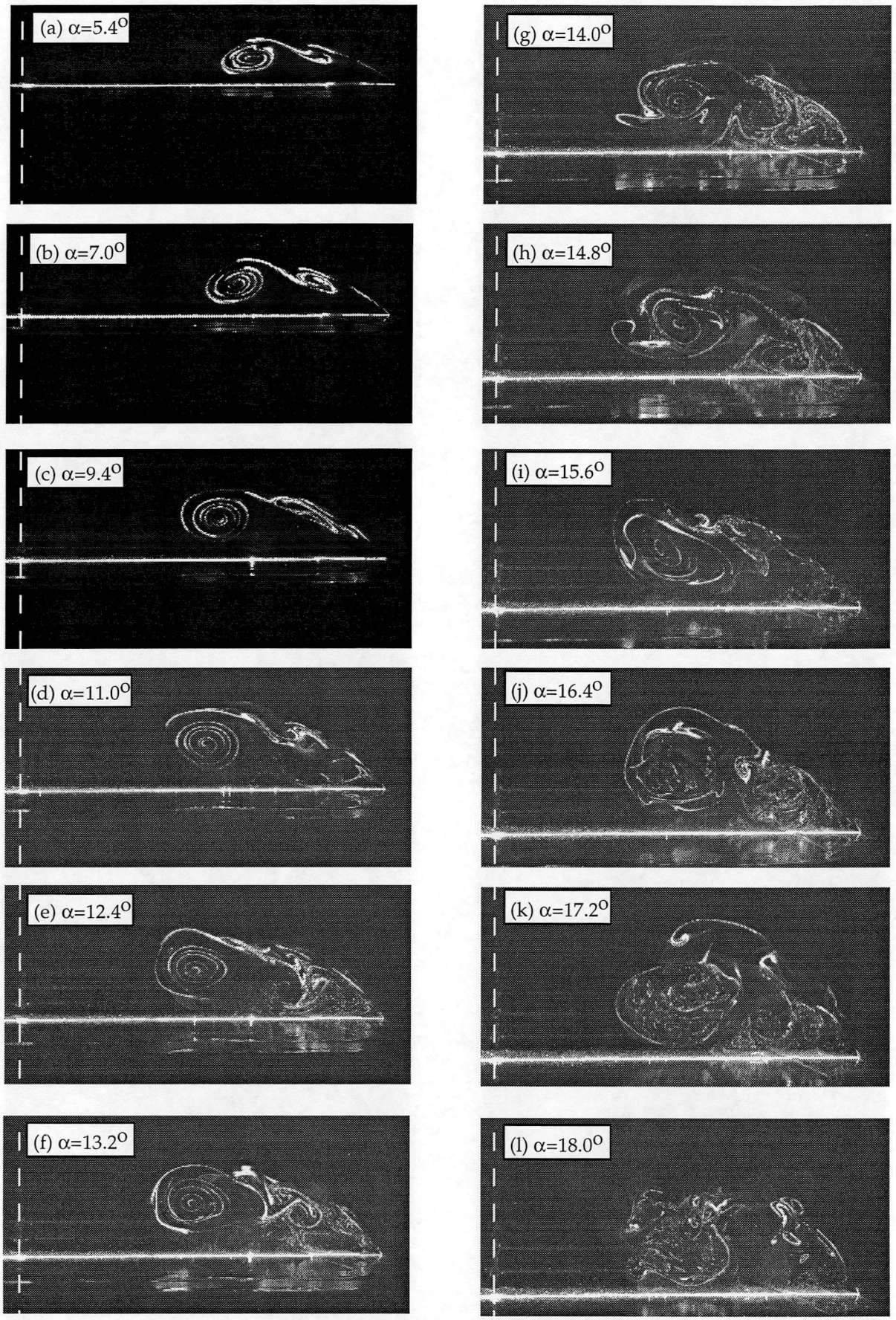

Figure 10 Sequence of images showing development of flow at k=0.014, x/c=0.8. The model incidence is indicated on each frame

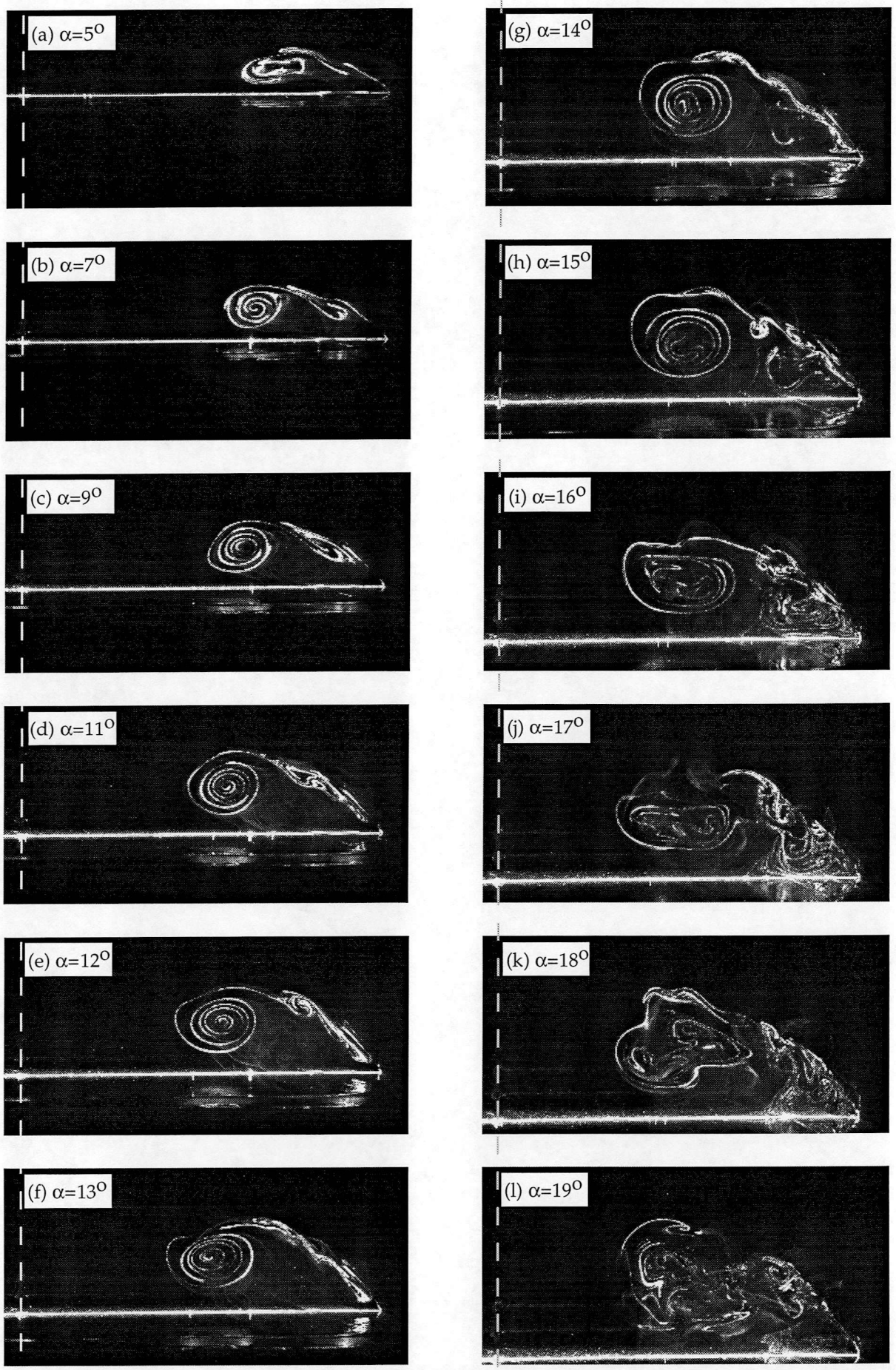

Figure 11 Sequence of images showing development of flow at k=0.035, x/c=0.8. The model incidence is indicated on each frame

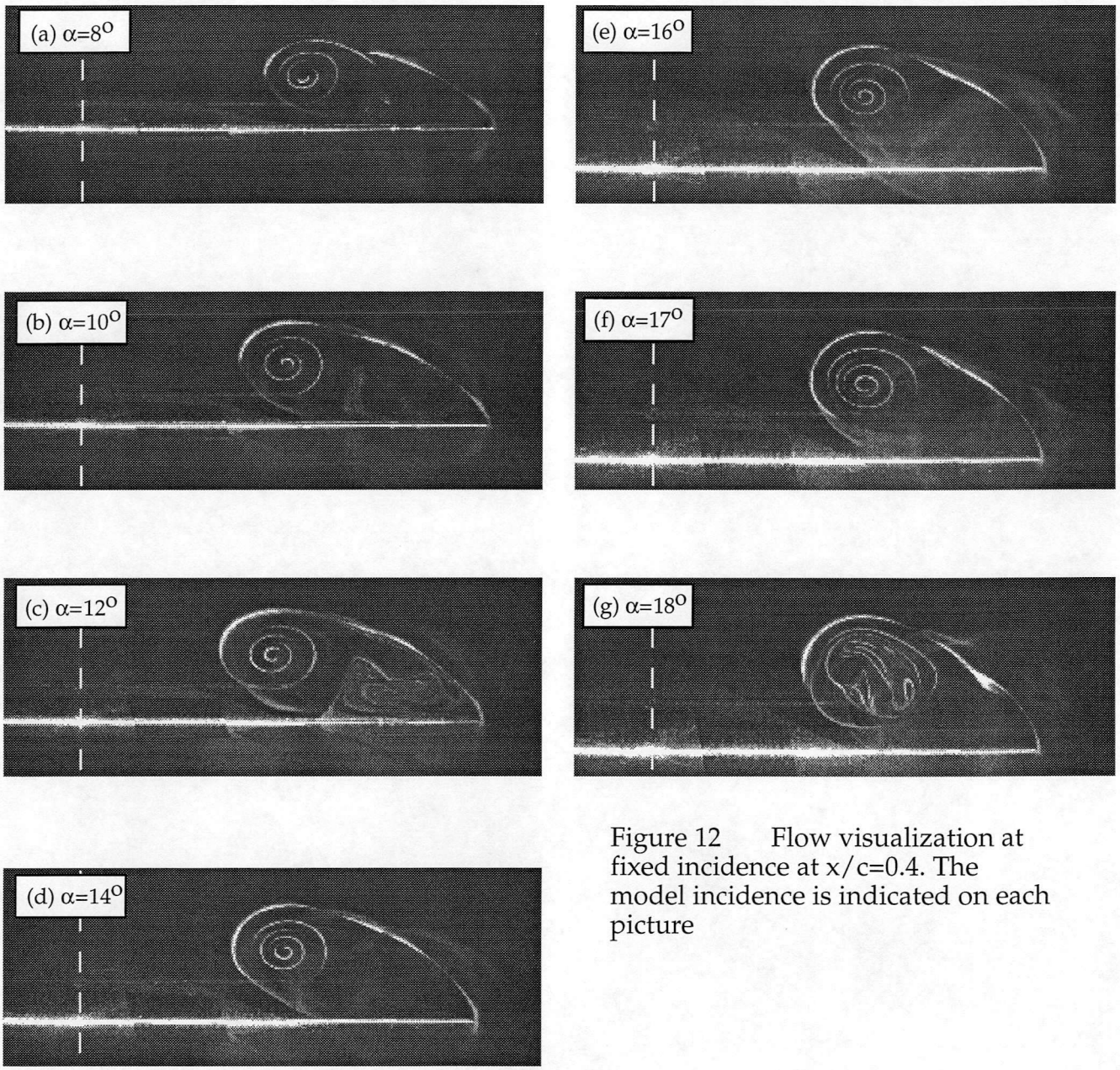

Figure 12 Flow visualization at fixed incidence at x/c=0.4. The model incidence is indicated on each picture

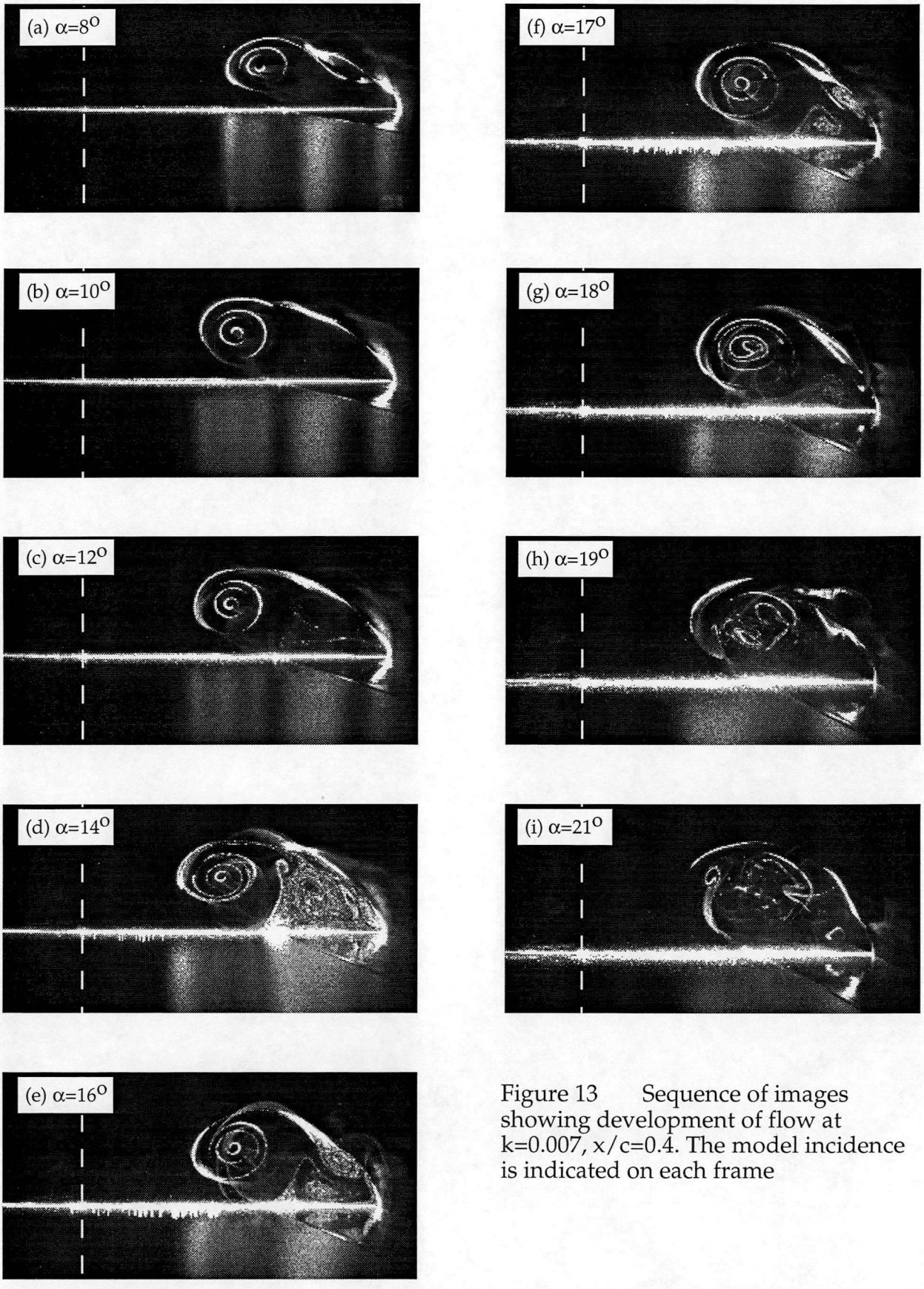

Figure 13 Sequence of images showing development of flow at k=0.007, x/c=0.4. The model incidence is indicated on each frame

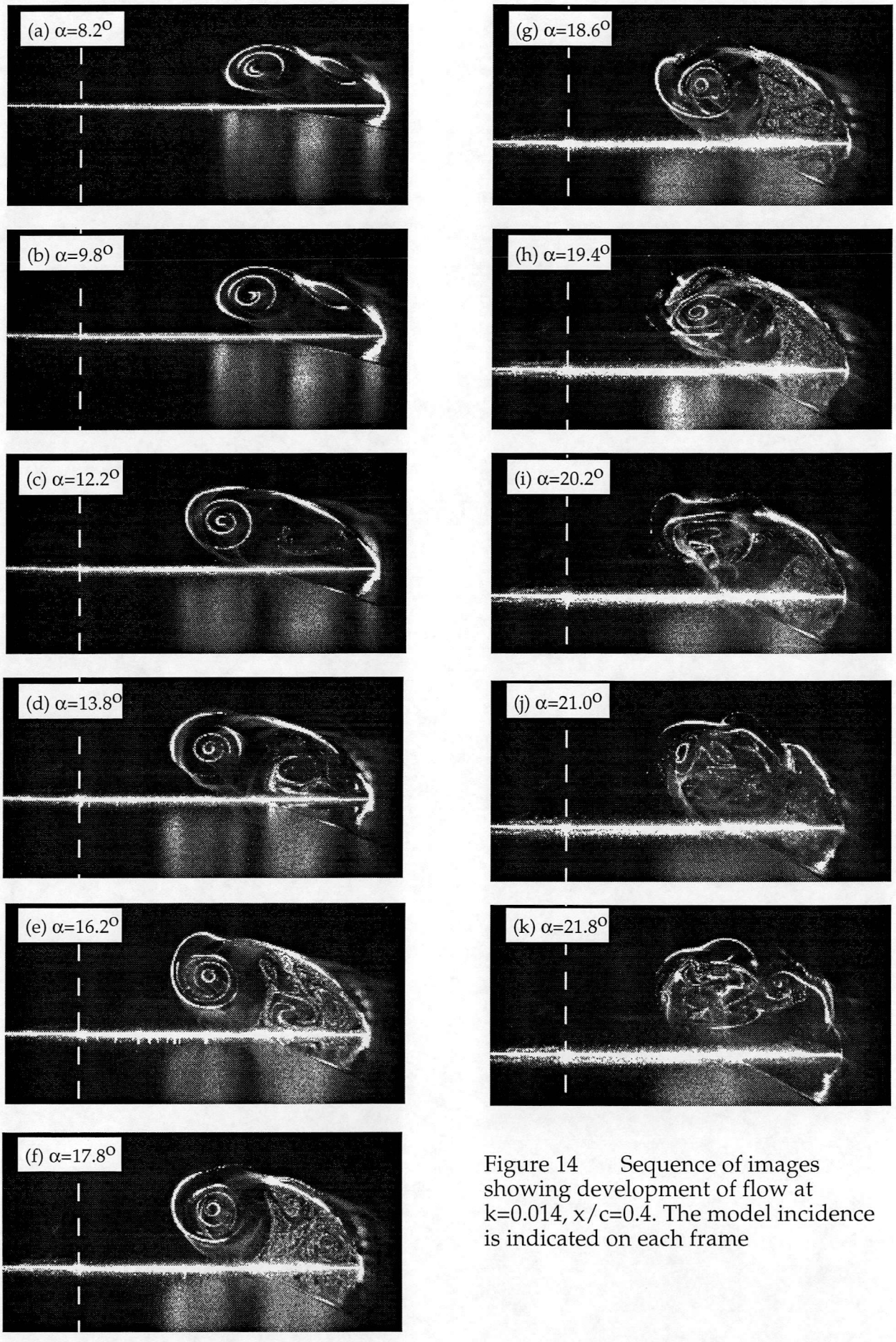

Figure 14 Sequence of images showing development of flow at k=0.014, x/c=0.4. The model incidence is indicated on each frame

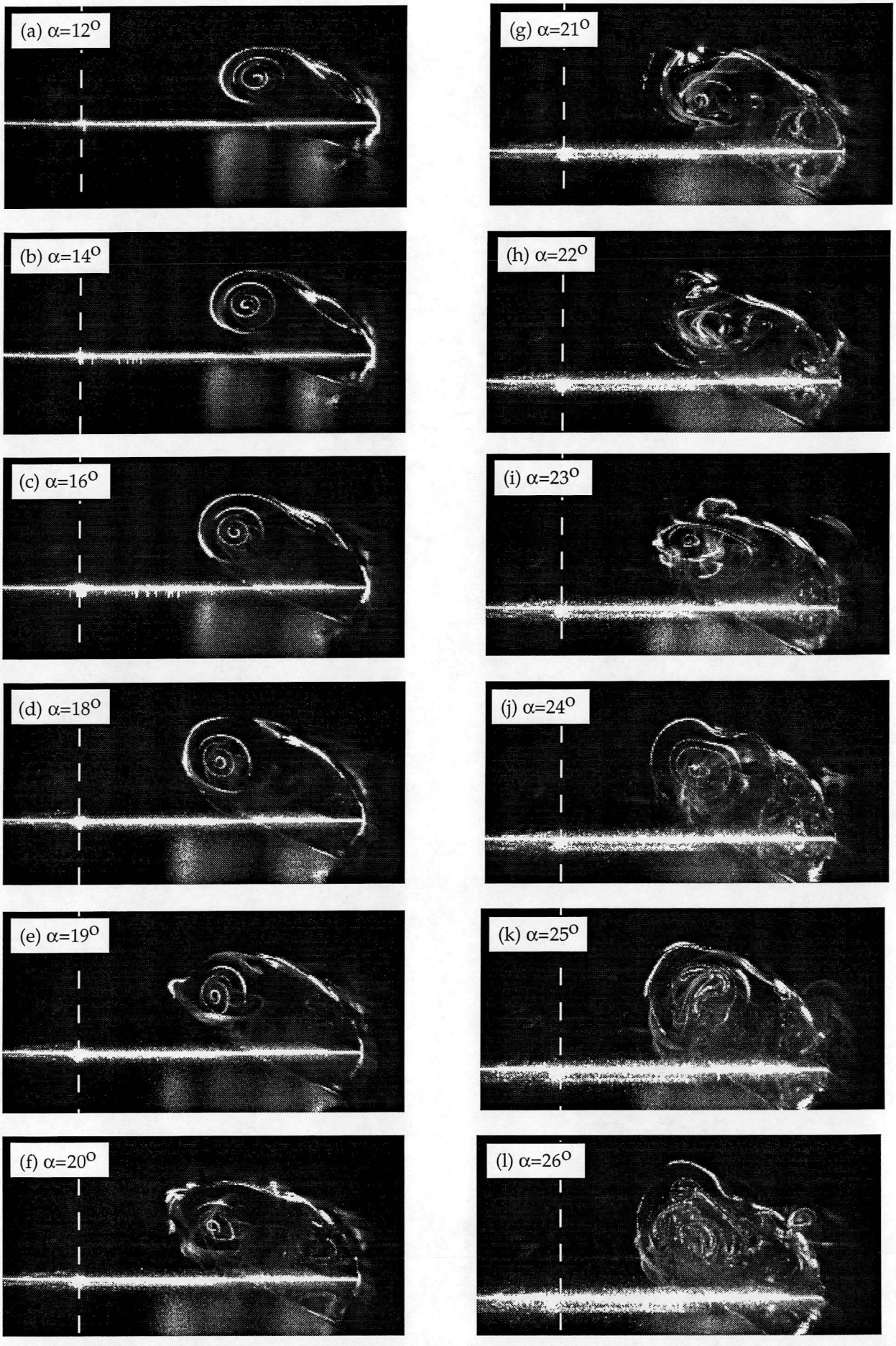

Figure 15 Sequence of images showing development of flow at k=0.035, x/c=0.4. The model incidence is indicated on each frame

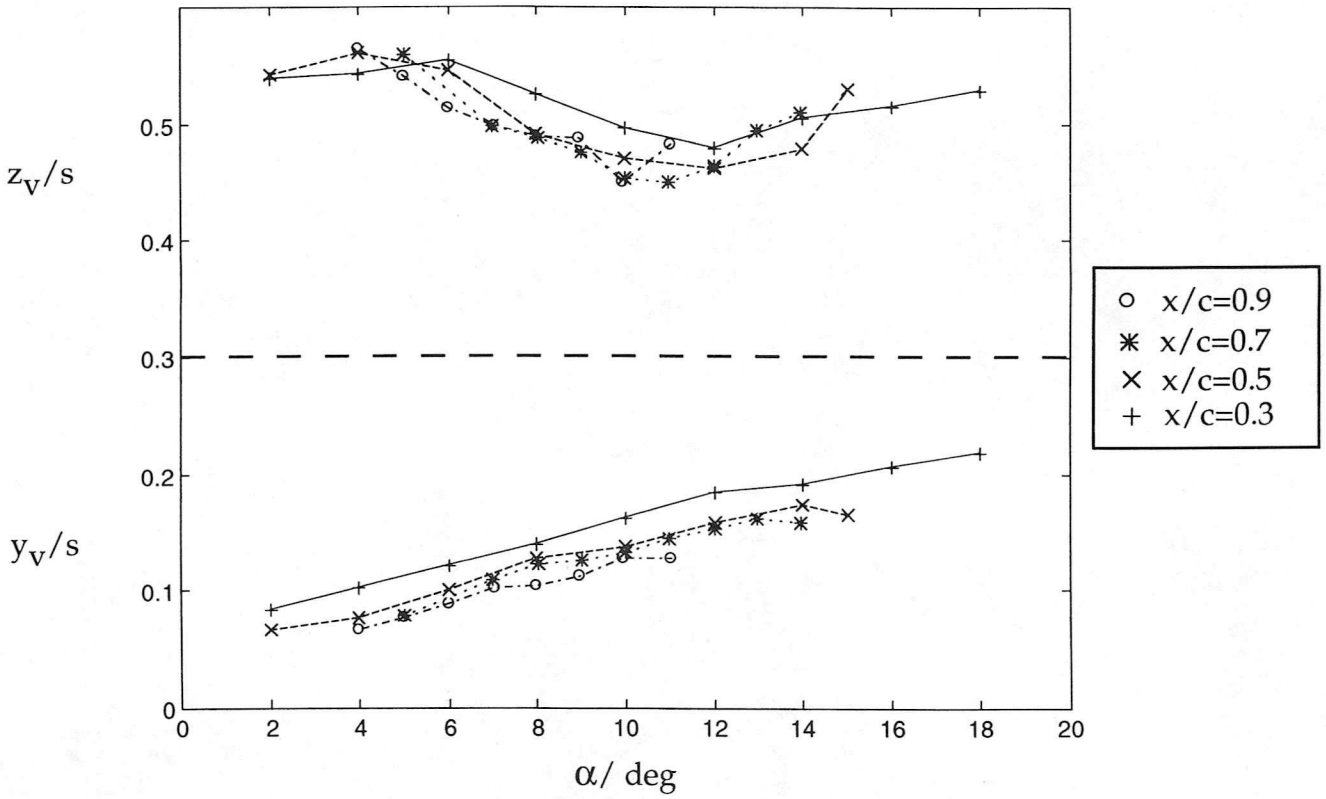

Figure 16a static tests

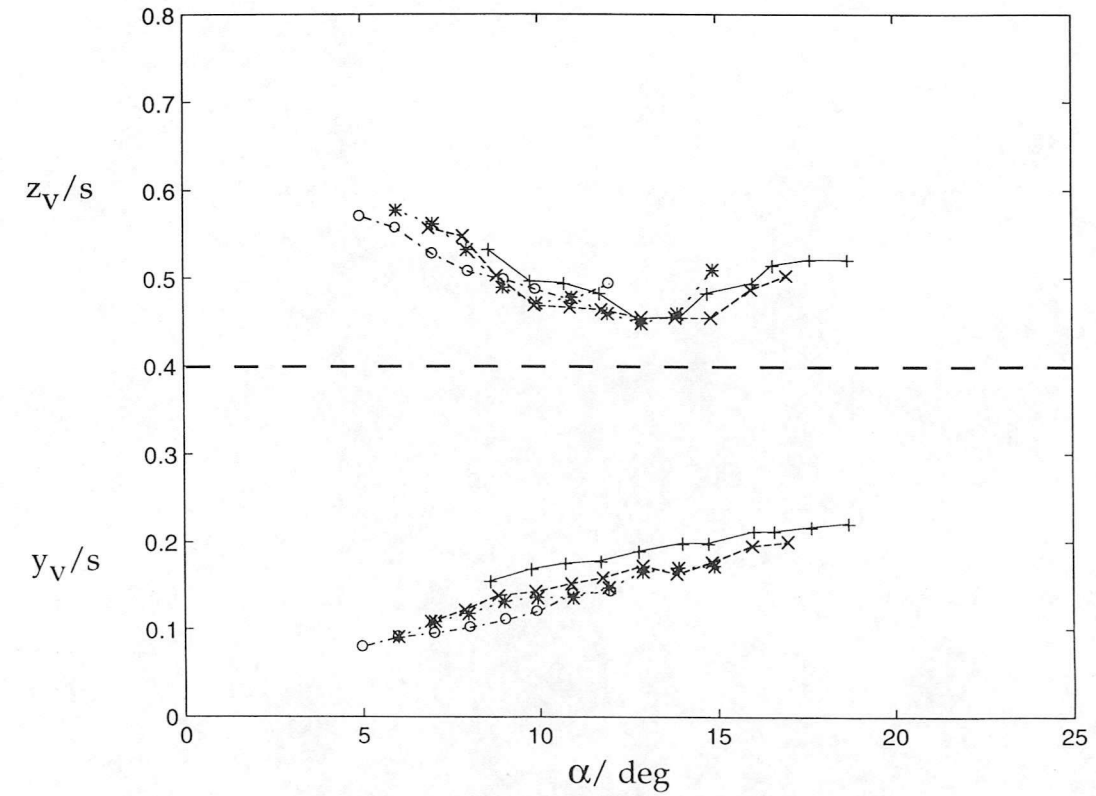

Figure 16b k=0.007

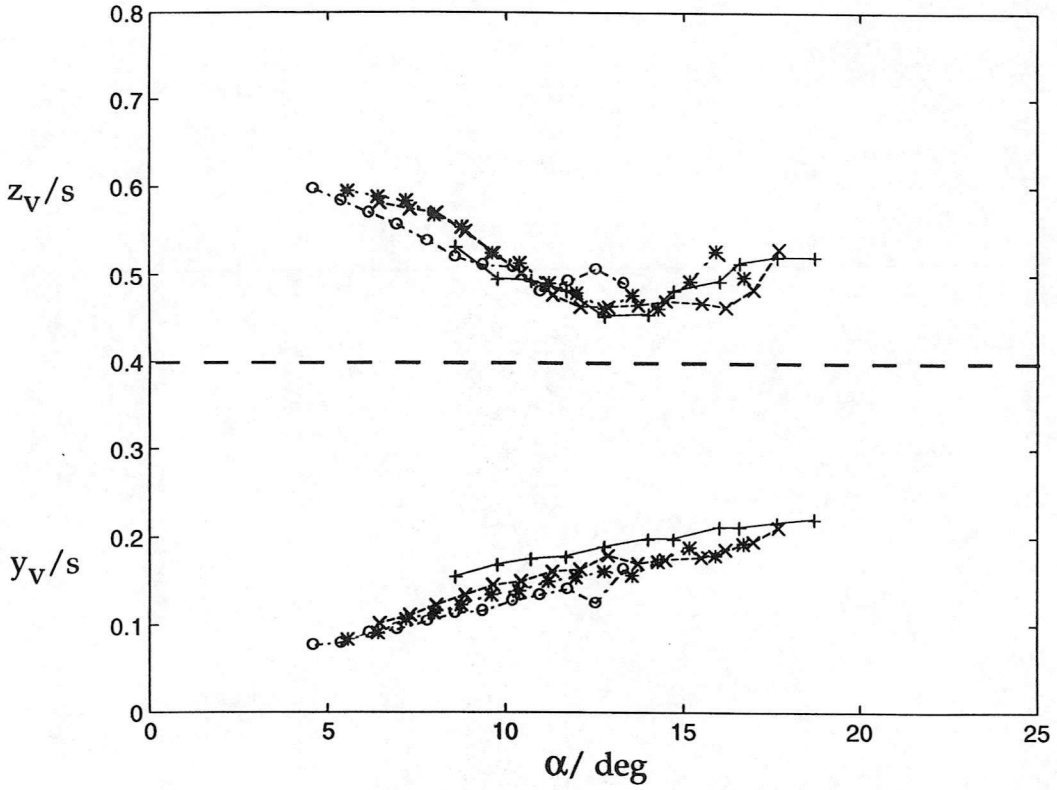

Figure 16c k=0.014

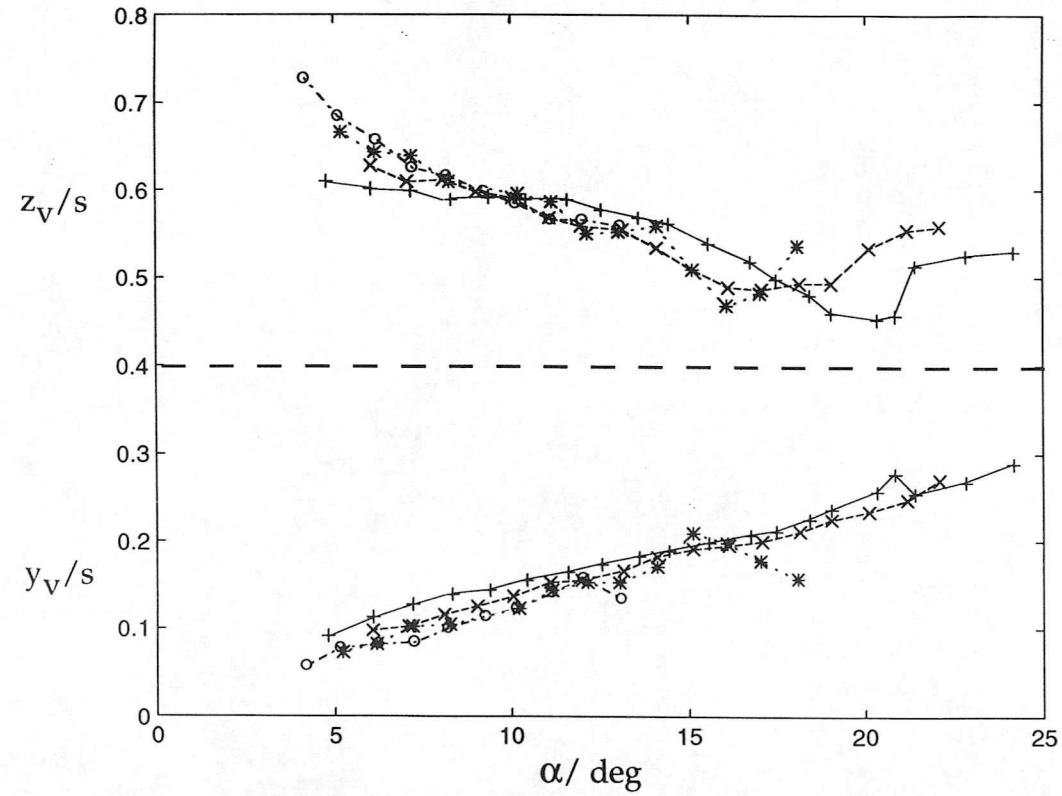

Figure 16d k=0.035

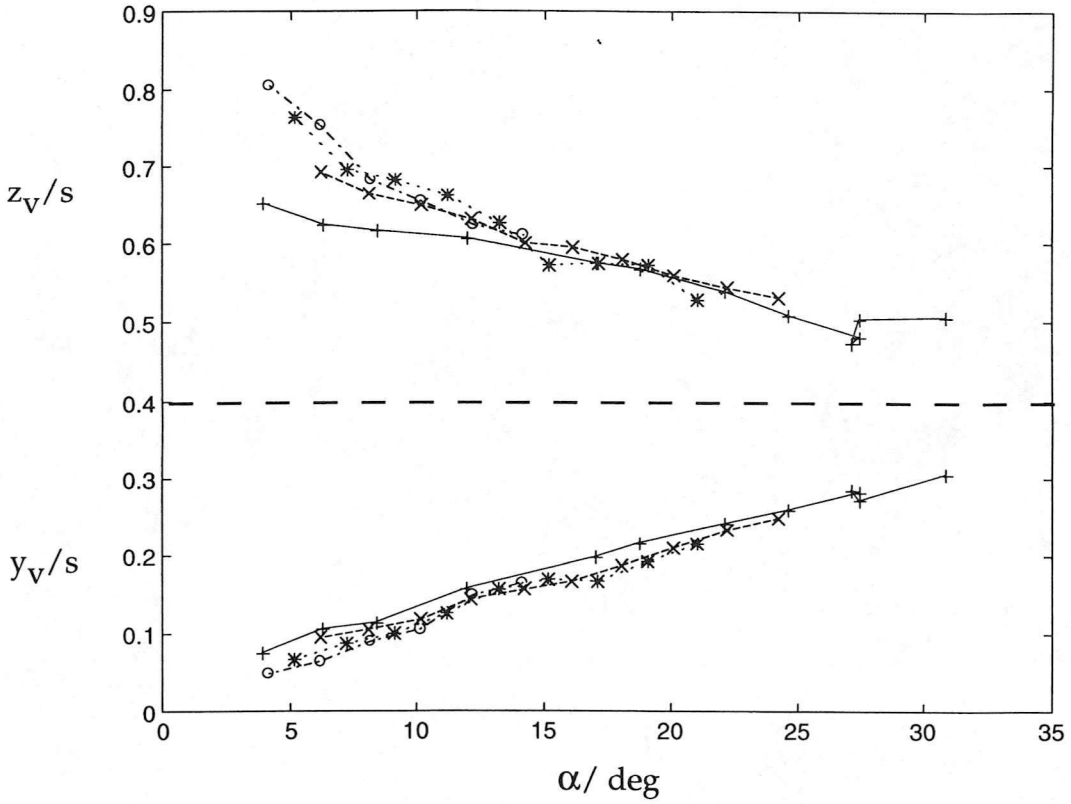

Figure 16e k=0.07

Figure 16 Vortex position variation with incidence as a function of chordwise position during ramp-up test. Each case represents a different pitch rate. The symbol key is indicated on figure 16a.

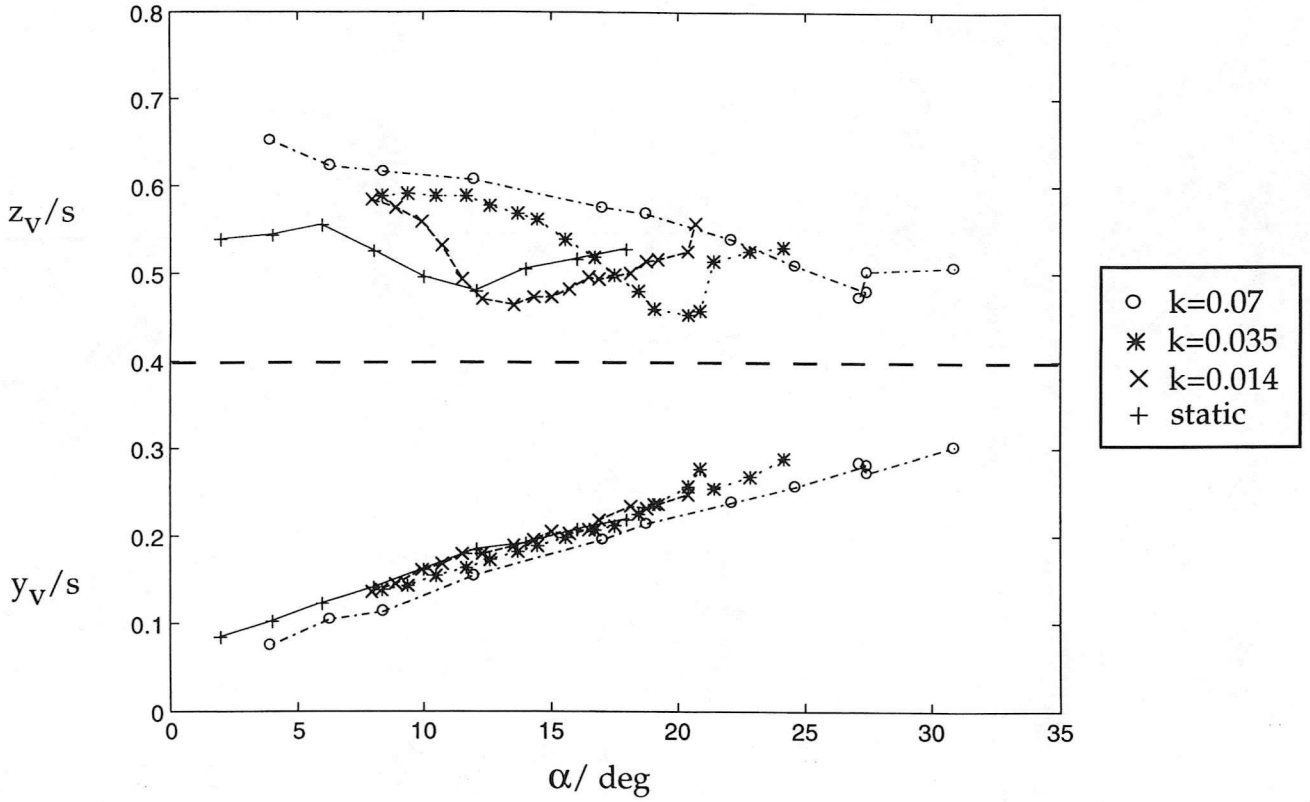

Figure 17a x/c=0.3

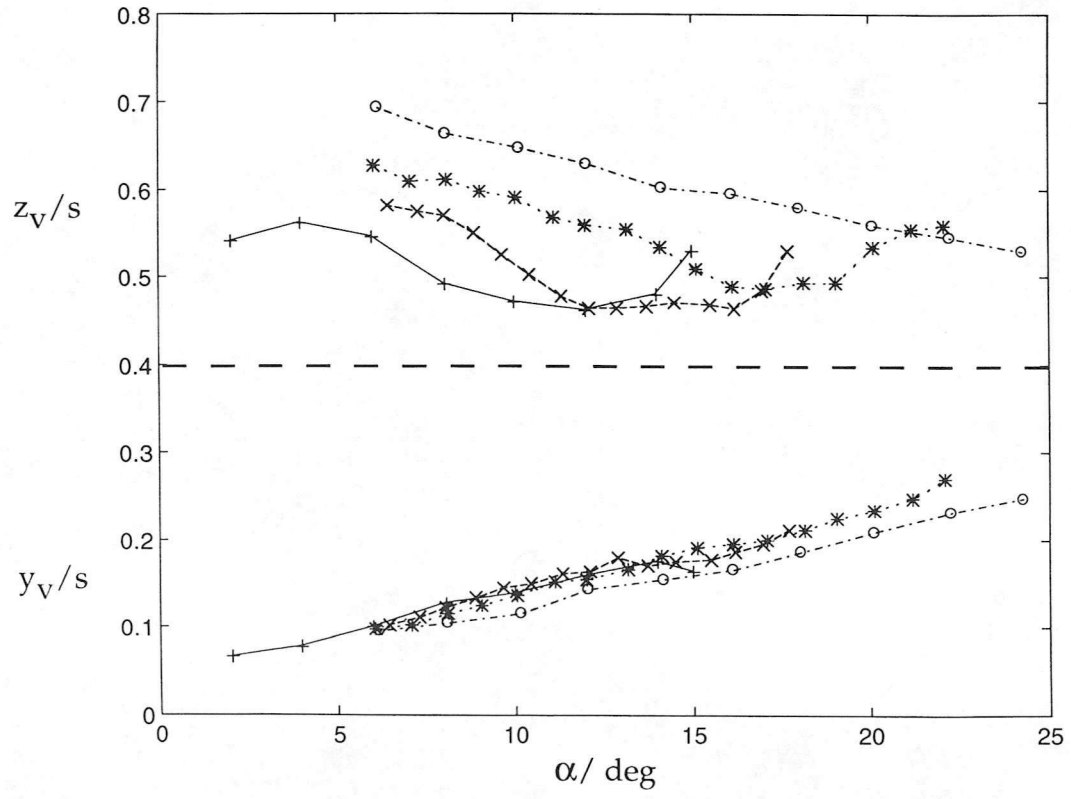

Figure 17b x/c=0.5

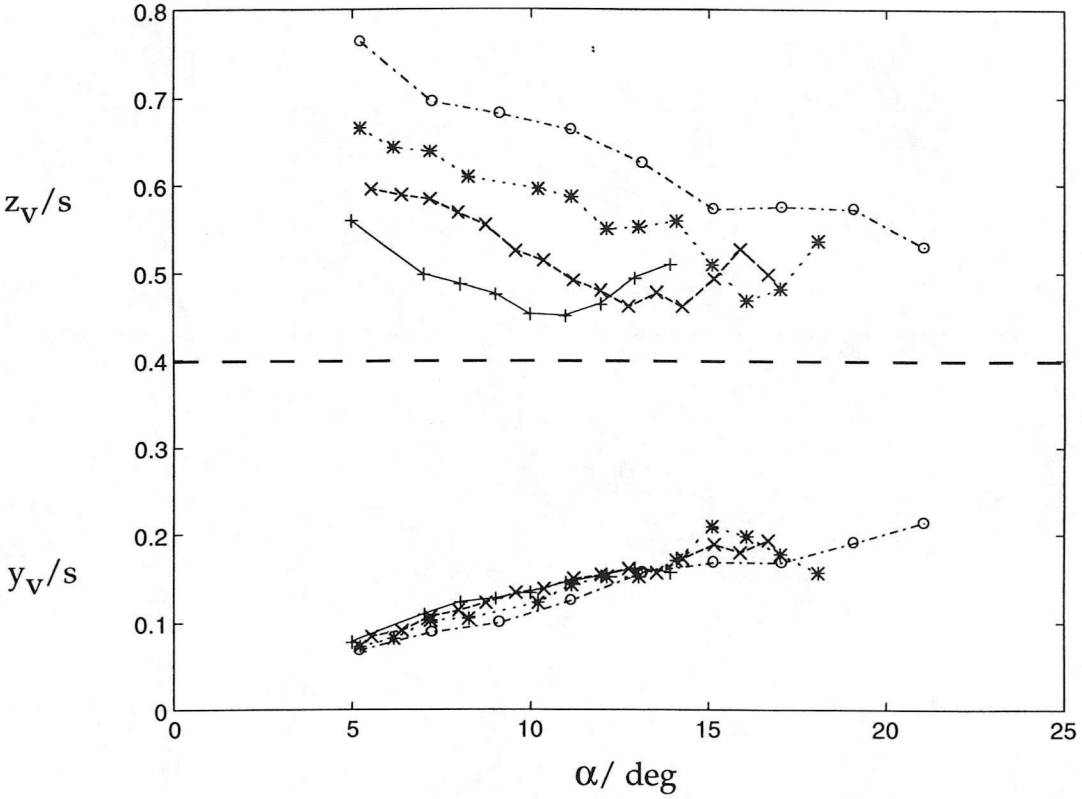

Figure 17c x/c=0.7

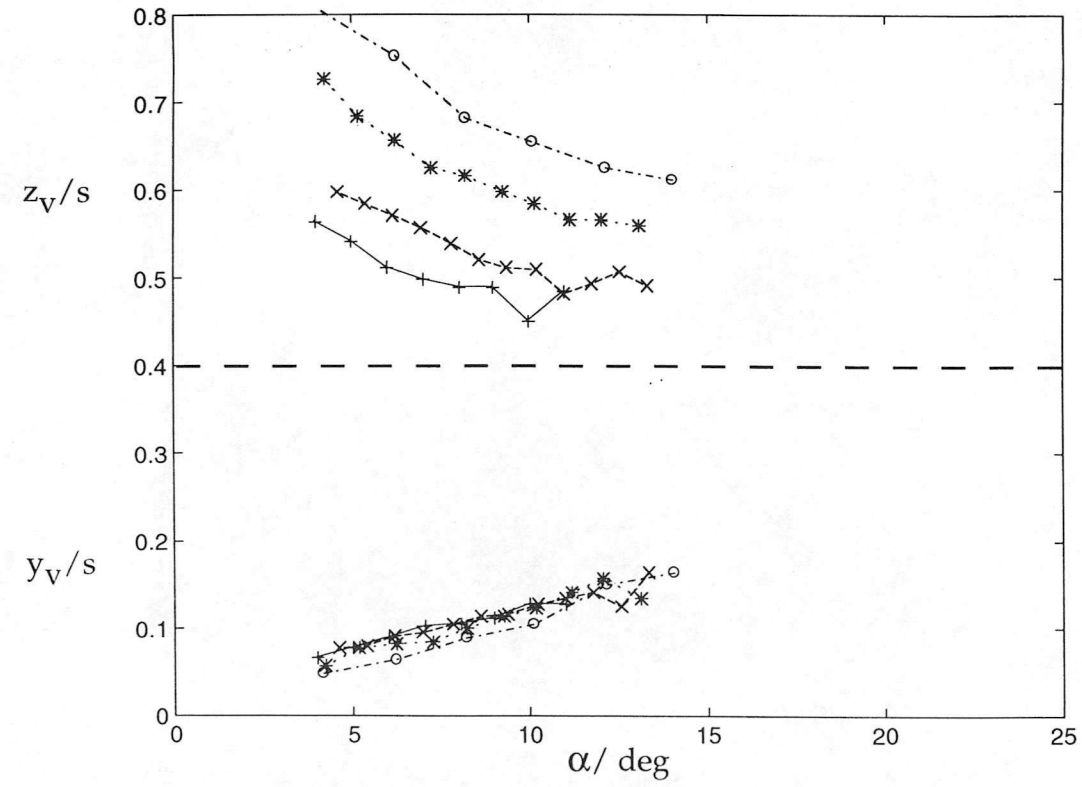

Figure 17d x/c=0.9

Figure 17 Vortex position variation with incidence as a function of pitch rate during ramp-up test. Each case represents a different chordwise position. The symbol key is indicated on figure 17a.

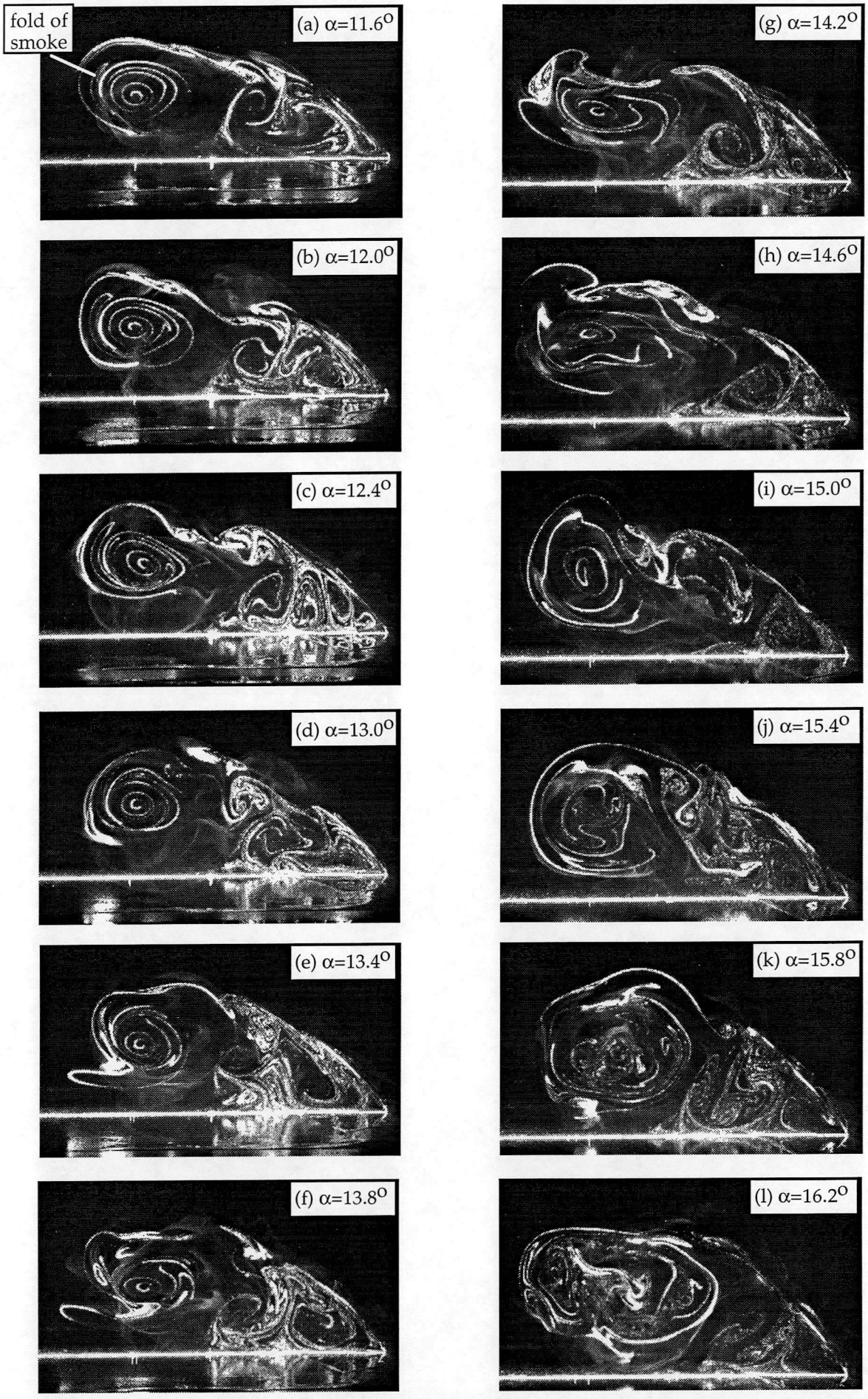

Figure 18 Detailed sequence of images showing vortex burst at k=0.014, x/c=0.8. The incidence is indicated on each frame.

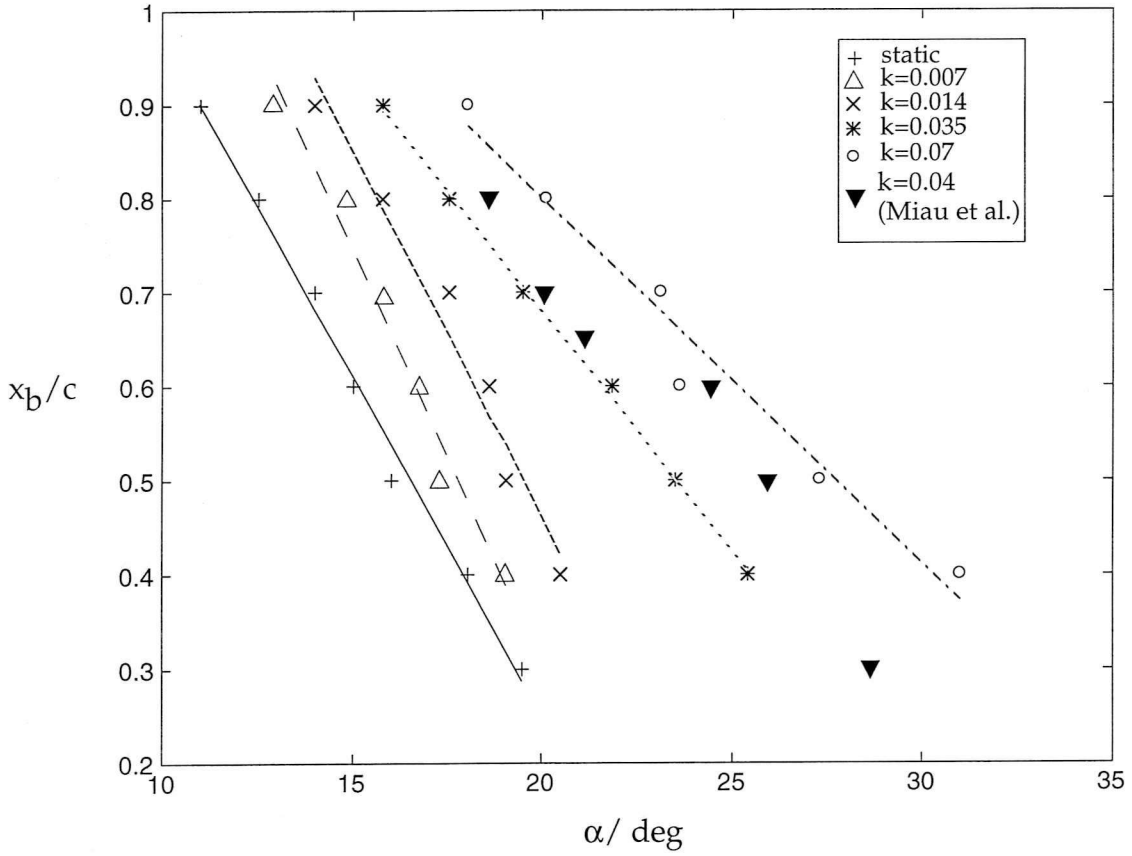

Figure 19a Progression of vortex breakdown with incidence as a function of pitch rate during ramp-up test.

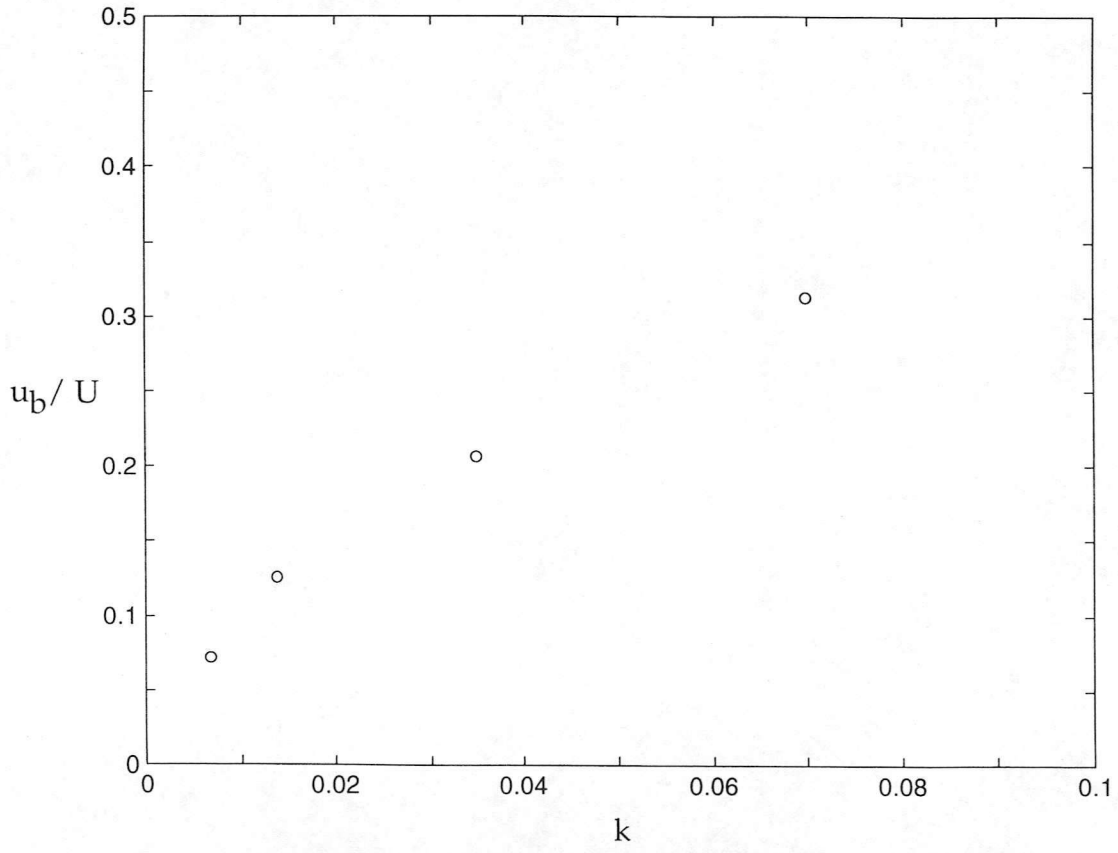

Figure 19b Burst progression speed as a function of reduced pitch rate during ramp-up test

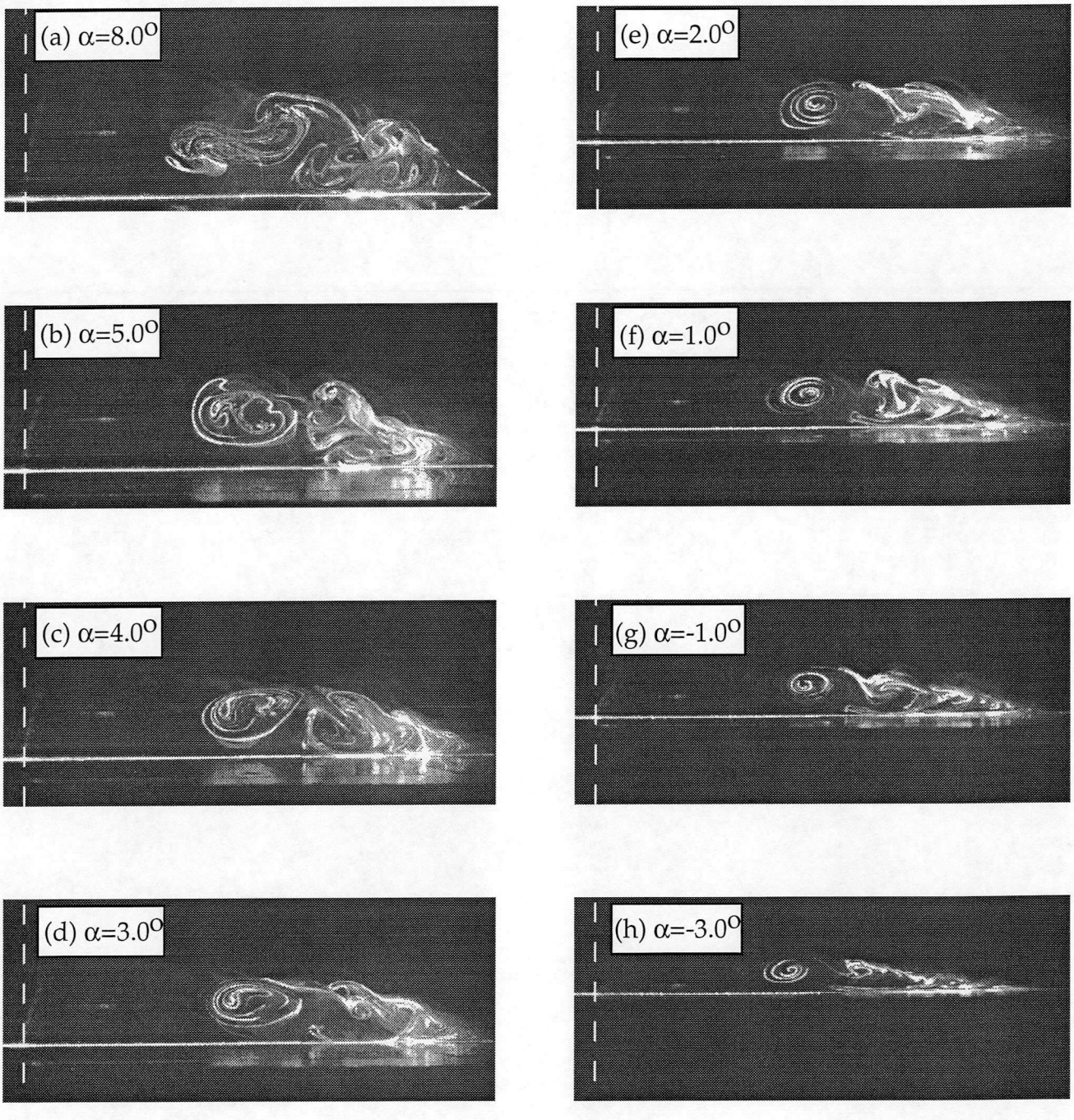

Figure 20 Sequence of images from a ramp-down test at k=-0.035. x/c=0.8. The incidence is indicated on each frame.

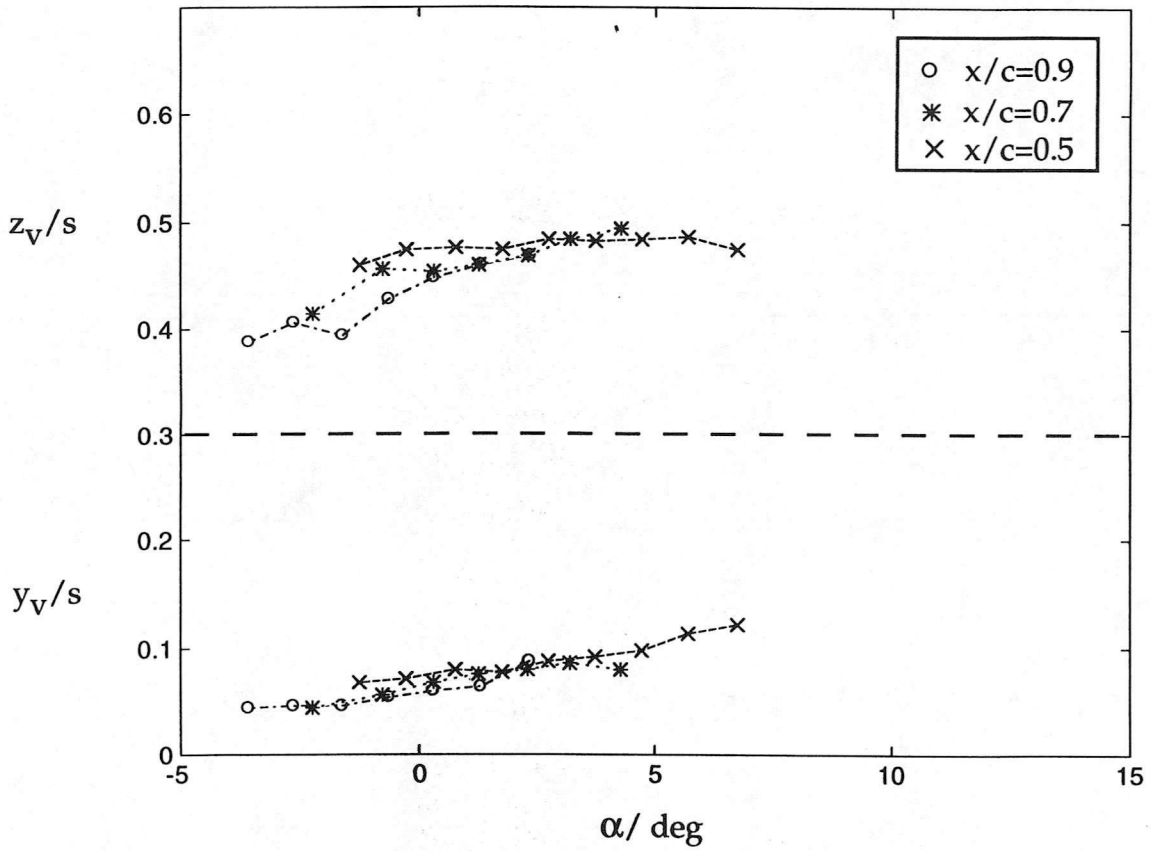

Figure 21a k=-0.035

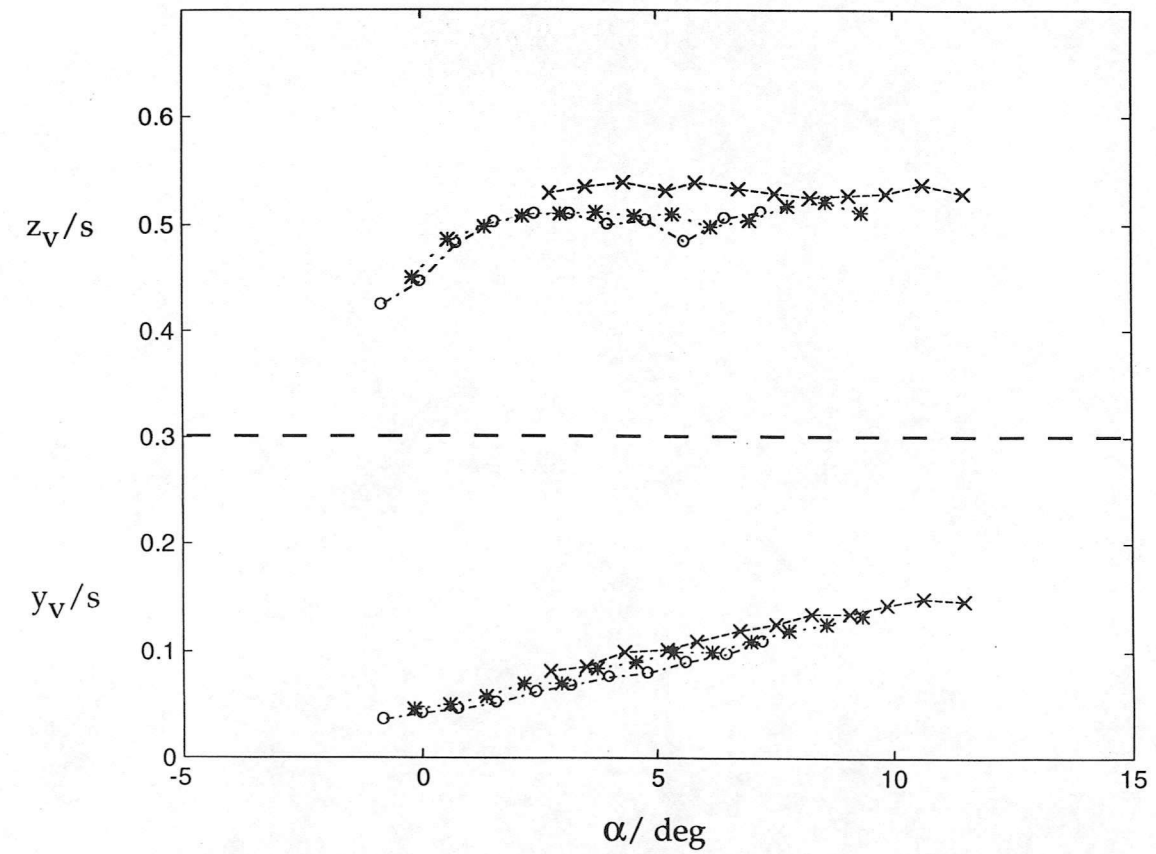

Figure 21b k=-0.014

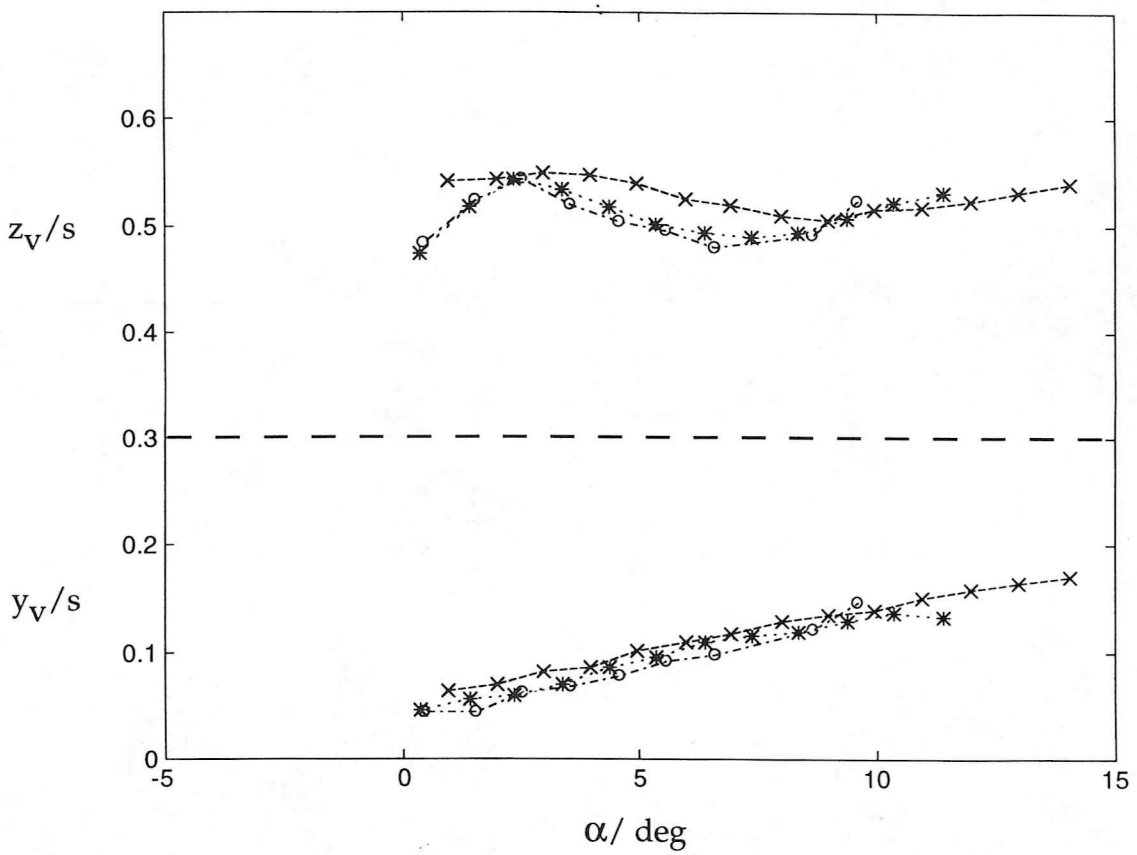

Figure 21c k=-0.007

Figure 21 Vortex position variation with incidence as a function of chordwise position during ramp-down test. Each case represents a different pitch rate. The symbol key is indicated on figure 21a.

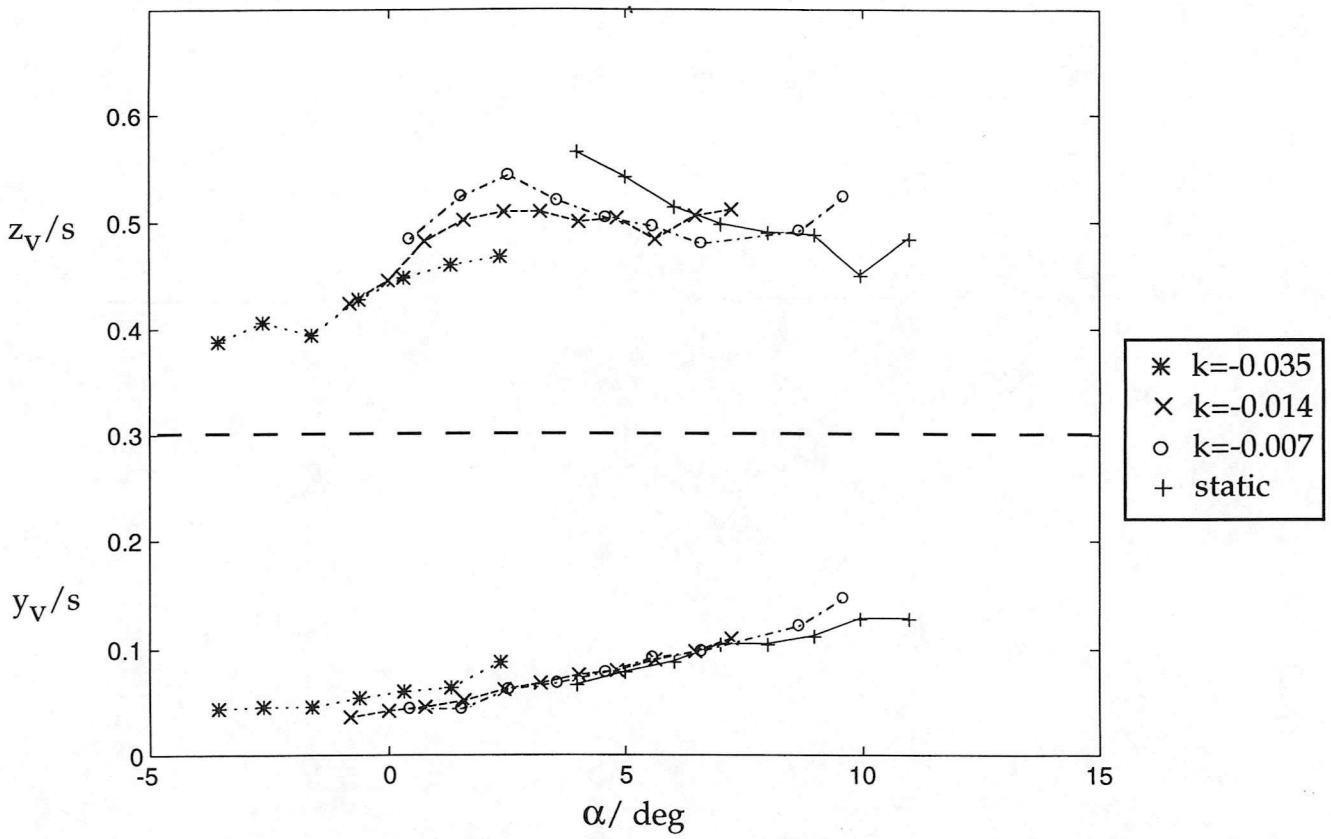

Figure 22a x/c=0.9

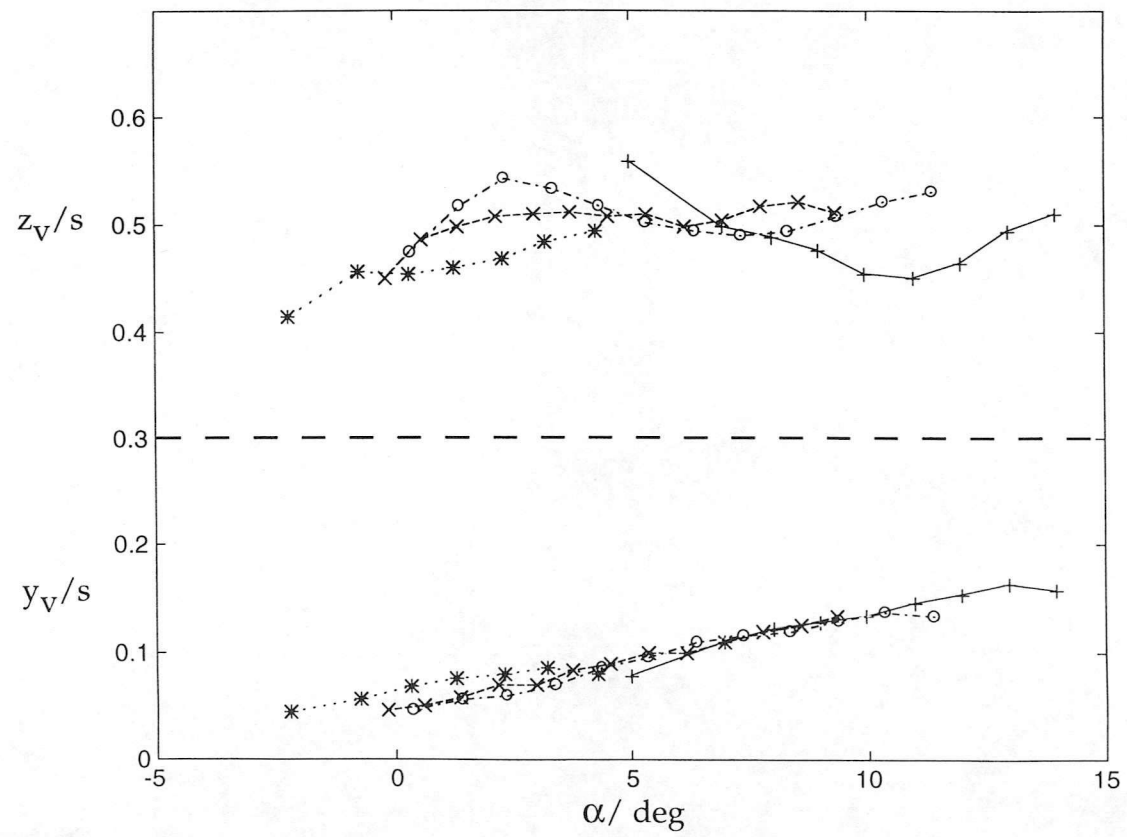

Figure 22b x/c=0.7

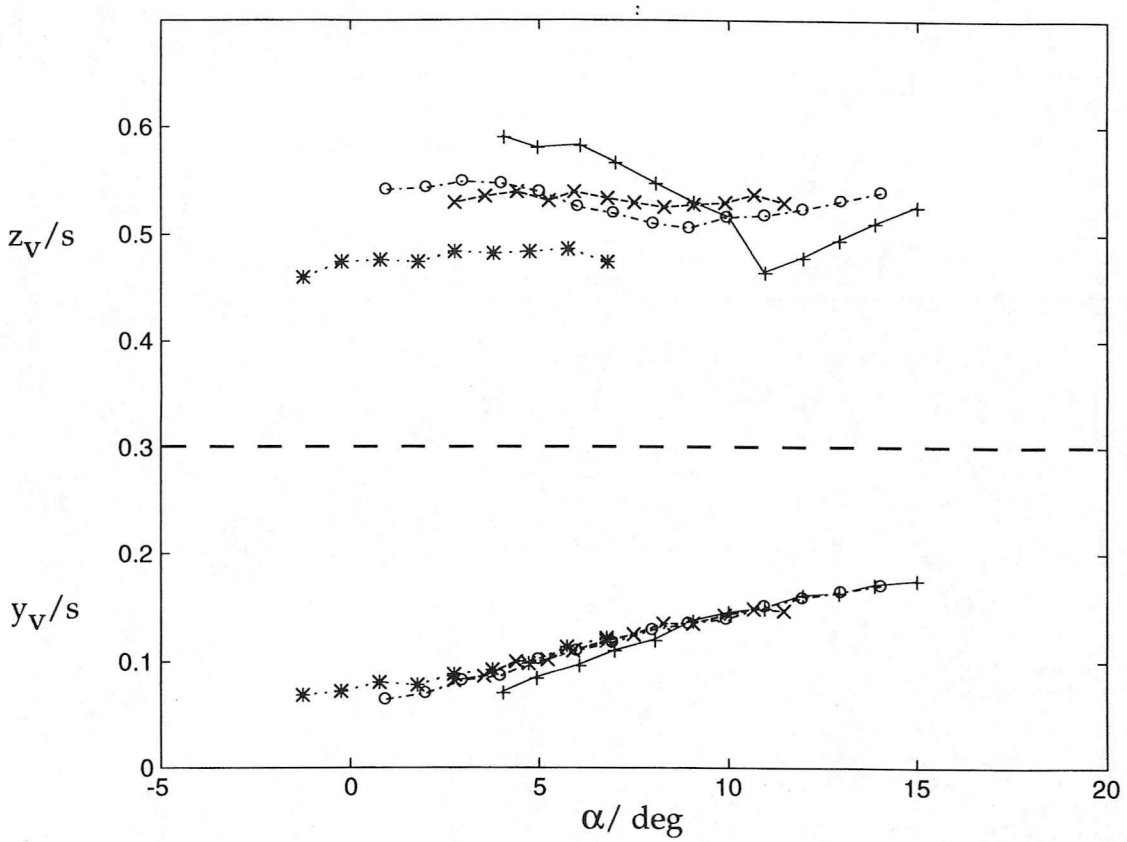

Figure 22c x/c=0.5

Figure 22 Vortex position variation with incidence as a function of pitch rate during ramp-down test. Each case represents a different chordwise position. The symbol key is indicated on figure 22a.

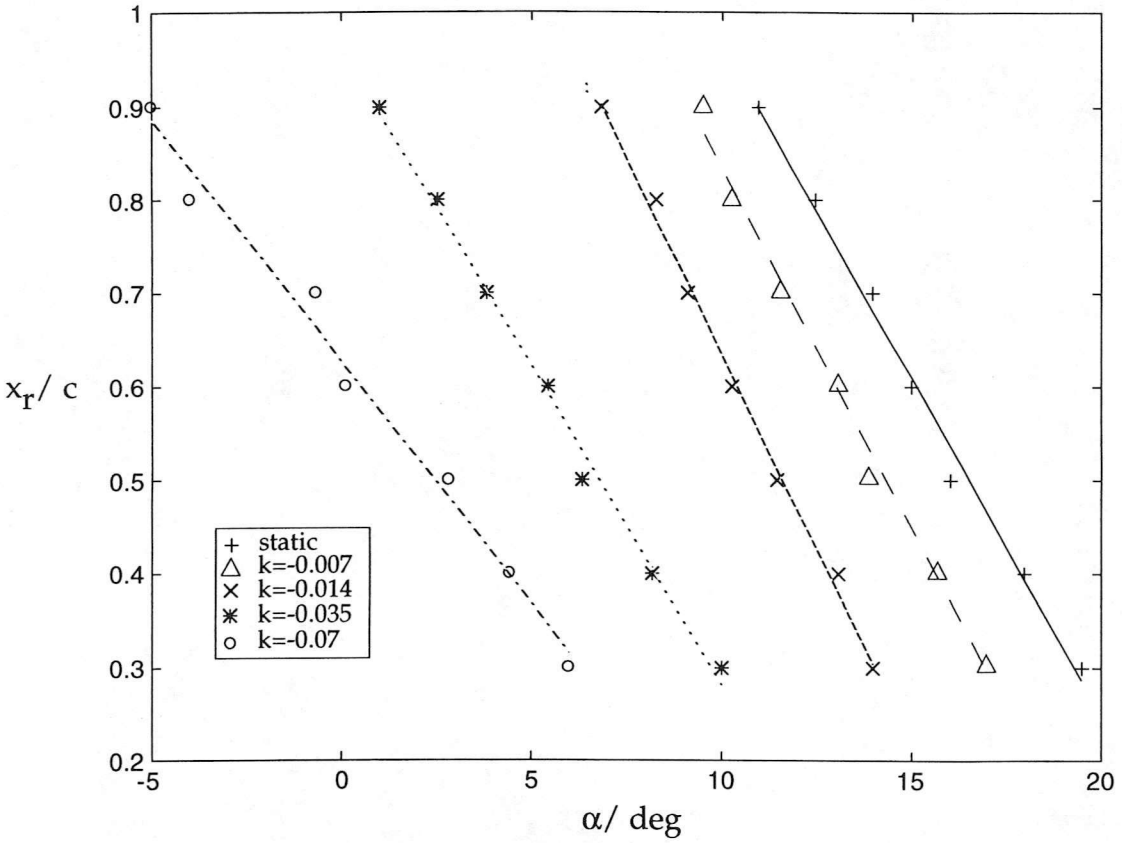

Figure 23a Vortex restoration progression with incidence as a function of pitch rate for ramp-down test.

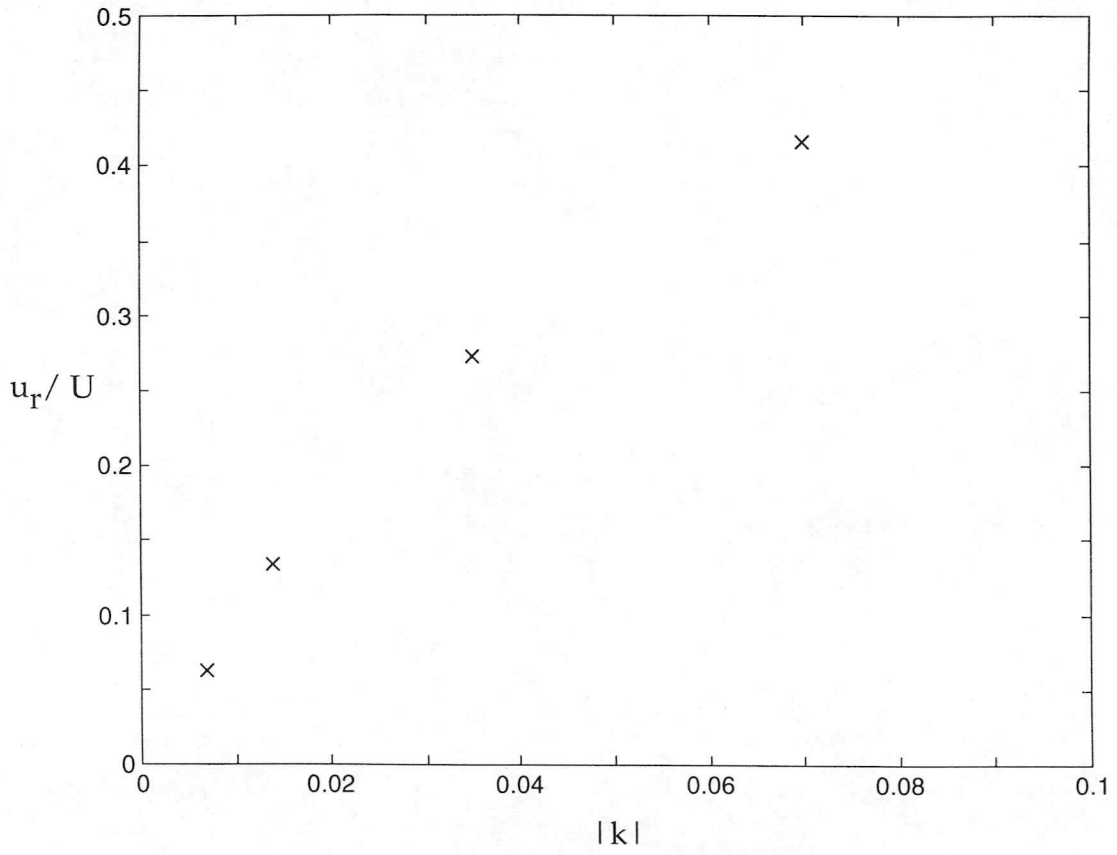

Figure 23b Restoration progression speed as a function of reduced pitch rate for ramp-down test

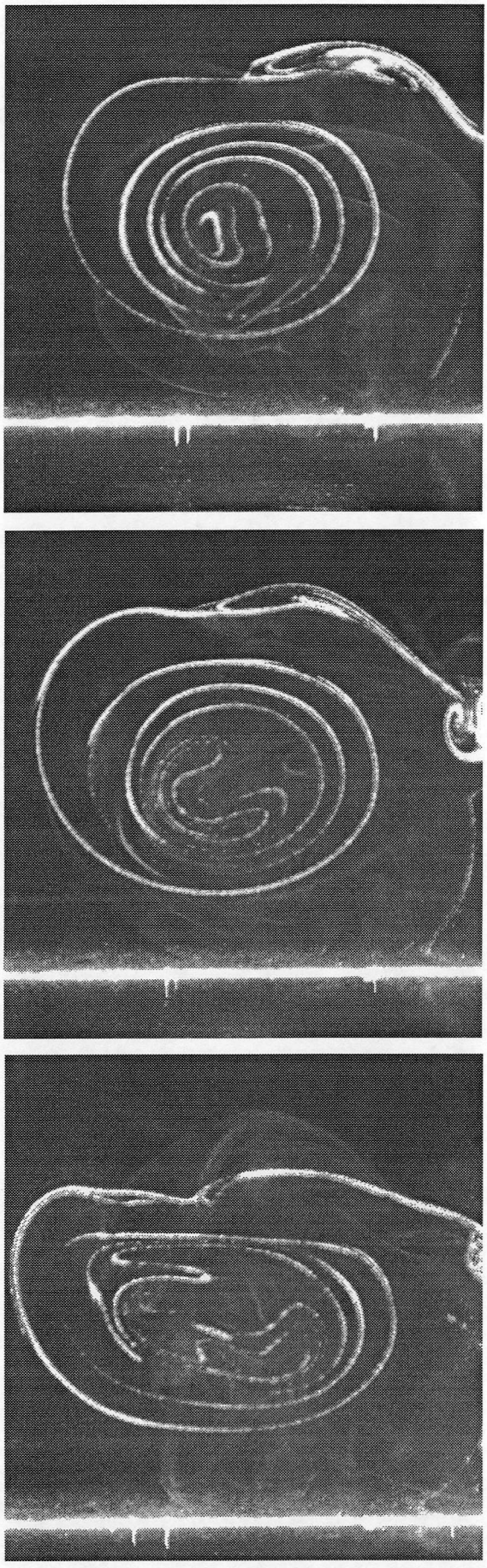

Figure 24 Close detail of vortex bursting . x/c=0.8, k=0.035

9. Appendix A: original proposal

1. AIMS

The aim of the proposed work is to provide a quality flow visualization of the unsteady flow around a pitching delta wing. Additionally a particle image velocimetry technique will be developed and applied to the measurement of the unsteady velocity field. The results will be of relevance to the design of helicopter rotor blade tips, and to unsteady flows encountered on modern civil aircraft.

2. BACKGROUND

Unsteady aerodynamics is a field of study finding continually increasing importance in the design of aircraft and rotorcraft. Historically the advent of the helicopter was the trigger for the first series of investigations in this field; in addition to influencing the design of the rotor blades, an understanding of the consequences of unsteady aerodynamics significantly affects the noise characteristics of the helicopter. The latter point is an important consideration when rotorcraft operate over urban environments. Fixed wing aircraft have only relatively recently benefited from knowledge of unsteady aerodynamics. To save fuel modern transport aircraft such as the Airbus family are unstable in flight. Thus to maintain the flight path a digital flight control system then actuates the aircraft control surfaces, and the effects of unsteady aerodynamics are found here. If the aircraft flies through a gust, the flight control system must compensate for the unsteady aerodynamic loads generated; incorrect understanding of the efffects of unsteady aerodynamics may therefore result in poor passenger comfort within the aircraft. Flow control devices, such as wing fences, vortex generators and strakes are all making an appearance on civil aircraft, and the powerful vortex structures that these produce may cause strong buffeting loads, which again encompasses the realm of unsteady aerodynamics. Finally, as unsteady aerodynamics finds application in all of man's aeronautical efforts, it is hardly surprising that animal flight has used the concepts to great advantage. The ability of the bumble bee to fly using the tiniest of wings is the most popular example, although it has only recently become clear exactly what the nature of the flow structures is.

The Department of Aerospace Engineering at the University of Glasgow has had a considerable research interest in unsteady aerodynamics for a number of years. The emphasis has been on helicopter problems (dynamic stall and dynamic reattachment of two and three dimensional wings performing pitching motion, and studies of helicopter blade-vortex interaction) and wind turbine applications. A recent project has been to provide unsteady aerodynamic test data relevant to the flow around helicopter blade tips. Blade tip flows affect the noise characteristics of the rotorcraft, and the aerodynamic and aeroelastic response of the whole blade. Furthermore the flow around the blade tip limits the maximum forward speed of the helicopter, and hence limits its versatility. Generally blade tips are no longer rectangular, but are swept and notched, and the presence of these features alters the formation of the tip vortices. Therefore the noise and aerodynamic performance of the whole blade is affected. The United Kingdom has a significant lead in helicopter blade tip technology, and hence a correct interpretation of the test data from the above project at Glasgow will contribute significantly to helicopter rotor blade design in this country.

The experimental techniques employed at the University of Glasgow have revolved around the use of a large number of pressure transducers placed below the skin of the test model. To aid the interpretation of the pressure data the Department has a wind tunnel (the smoke tunnel) specially designed for flow visualization. Models are placed in this wind tunnel, and are subjected to rapid pitching motion with the aid of a stepper motor. The subsequent flow patterns shown by smoke filaments are then recorded using video or conventional photography.

The proposed research is to perform a detailed flow visualization of the unsteady vortex flows around a pitching delta wing. This will make a contribution to the above programme, and will also serve as a natural progression to the proposer's research work prior to taking up the lecturing post. In addition it will allow him to develop experimental techniques used as a postgraduate student that he has not since had the opportunity to use. The research would not only provide a valuable insight into the behaviour of unsteady vortex flows, but would develop a valuable facility for further research within the Department.

3. METHODOLOGY

Smoke flow visualization

When smoke is used to visualize delta wing flows, it has to be injected at the correct location within the flow field. Smoke injected into the flow upstream of the model takes a long time to be entrained into the growing vortices, and hence leads to a significant ambiguity in the interpretation of the flow patterns. If the smoke is injected into the boundary layer on the windward surface of the model, however, the presence of the vortices is immediately revealed. When smoke is injected into the flow in this way, any vibration from the actuation system disturbs the smoke. Hence successful visualization of the flow requires refinement of the pitching apparatus, principally by the use of a higher quality, vibration free actuator than is presently available to the Department. Funds are required for the purchase of this item.

Use of Particle Image Velocimetry technique

Although smoke flow visualization is a very important experimental technique it yields virtually no information on the velocity and vorticity fields of a flow. These data are of crucial importance in understanding the fluid flow mechanisms. In steady flows the velocity field may be determined by traversing a single point measuring probe across the velocity field. However, the highly separated, unsteady nature of pitching delta wing flows necessitates an experimental technique that can allow instantaneous velocity measurement over a large portion of the velocity field. Particle image velocimetry (PIV) offers such a capability. In this method the flow is seeded with microscopic particles. These are then illuminated, often using laser light, and the particle motion is photographed. Illumination over a wide area using a laser is best done by reflecting the laser beam off a rapidly-spinning, multi-faceted mirror. Since the laser beam is scanning across the flow field many times per second, then a trace of a particle on a photographic emulsion appears as a series of dots, and the distance between the dots is proportional to the particle velocity, and hence the fluid velocity. To measure the velocity vectors the photographic negative has to be scanned into a computer. Processing techniques (typically fast Fourier transforms) are then applied to the image. This is a very computationally intensive task, owing to the enormous amount of data on each negative. Once the fluid velocity field is known then the vorticity field is determined by differentiation. The Department already has an Argon ion laser of moderate power, photographic equipment and a 35mm slide scanner, which would all find application in this part of the proposed work. Additional items required for the execution of the research are the multi-faceted mirror, a fast acting electro-mechanical shutter to assist with the photography, and a dedicated, desk-top computer for the image analysis.

As a final note the above improvements to the flow visualization facility, and the development of the PIV technique will serve as a valuable asset to the proposer's research interests well beyond the period of the current proposal. The above techniques find application in all areas of fluid mechanics, and PIV has the advantage that the same processing algorithms can be applied to data from different wind tunnels. Hence this capability would allow ready application of the same techniques in different facilities, and would thus enhance the Department's research capabilities.